

*work with letter dtd 9/18/97*

**MODELING FAULT-DIKE INTERACTION:  
IMPLICATIONS FOR LATERAL DIVERSION  
OF DIKES AND ALIGNMENT OF VOLCANOES  
IN THE YUCCA MOUNTAIN  
(NEVADA) REGION**

*Prepared for*

**Nuclear Regulatory Commission  
Contract NRC-02-93-005**

*Prepared by*

**D.A. Ferrill  
C.B. Connor  
J.A. Stamatakos  
H.L. McKague  
B.E. Hill  
G.I. Ofoegbu  
R. Terhune**

**Center for Nuclear Waste Regulatory Analyses  
San Antonio, Texas**

**September 1997**

# CONTENTS

Section	Page
FIGURES . . . . .	v
ACKNOWLEDGMENTS . . . . .	vii
QUALITY OF DATA, ANALYSES, AND CODE DEVELOPMENT . . . . .	vii
1 INTRODUCTION . . . . .	1-1
2 INDICATIONS OF FAULT-DIKE INTERACTION NEAR YUCCA MOUNTAIN . . . .	2-1
3 THEORETICAL CONSIDERATIONS . . . . .	3-1
4 ANALYTICAL MODELING . . . . .	4-1
4.1 CRACK TIP CONSIDERATIONS . . . . .	4-1
4.2 GEOMETRIC CONSIDERATIONS . . . . .	4-1
4.2.1 Model Constraints . . . . .	4-1
4.2.2 Results . . . . .	4-2
5 NUMERICAL MODELING RESULTS . . . . .	5-1
6 <i>IN SITU</i> STRESS AND FAULT-DIKE INTERACTION AT YUCCA MOUNTAIN . . . .	6-1
7 VOLCANO ALIGNMENTS . . . . .	7-1
8 CONCLUSIONS . . . . .	8-1
9 REFERENCES . . . . .	9-1
APPENDIX	

## FIGURES

Figure		Page
1-1	Schematic models of fault-dike interaction in profile . . . . .	1-2
1-2	Lateral diversion distance ( $d$ ) is defined as a function of the vertical distance of dike capture by a fault ( $h$ ), and the dip of the fault ( $\alpha$ ) . . . . .	1-3
1-3	Graphical illustration of the amount of lateral diversion of a dike ( $d$ ) once dike capture has occurred given the vertical distance of dike capture ( $h$ ) and fault dip ( $\alpha$ ) . . . . .	1-3
4-1	Summary diagram from analytical modeling of fault-dike interaction (after Connor et al., 1993; McDuffie et al., 1994) illustrating theoretical thresholds between vertical dike propagation versus fault intrusion . . . . .	4-3
5-1	Summary diagram from analytical modeling of fault-dike interaction (figure 3) with results of numerical dynamic analyses illustrated using dots . . . . .	5-2
6-1	Dilation tendency plot for the Yucca Mountain area in present day stress field (stress field from Ferrill et al., 1996b and Morris et al., 1996) . . . . .	6-2
6-2	Cross sections through Crater Flat and Bare Mountain showing two alternative interpretations for fault geometries. . . . .	6-3
7-1	Conceptual block diagrams of potential structural control on volcanism . . . . .	7-2

## ACKNOWLEDGMENTS

This report was prepared to document work performed by the Center for Nuclear Waste Regulatory Analyses (CNWRA) for the Nuclear Regulatory Commission (NRC) under Contract No. NRC-02-93-005. The activities reported here were performed on behalf of the NRC Office of Nuclear Material Safety and Safeguards (NMSS) and the Office of Nuclear Regulatory Research. The report is an independent product of the CNWRA and does not necessarily reflect the views or regulatory position of the NRC.

### QUALITY OF DATA, ANALYSES, AND CODE DEVELOPMENT

**DATA:** CNWRA-generated original data contained in this report meets quality assurance requirements described in the CNWRA Quality Assurance Manual. Sources for other data should be consulted for determining the level of quality for those data.

**ANALYSES AND CODES:** 3DStress<sup>®</sup> Version 1.2 was used for analyses contained in this report. The 3DStress computer code is controlled under the CNWRA Software Configuration Procedures. DYNA3D was used for analyses contained in this report (appendix A). The DYNA3D code is not controlled under the CNWRA software configuration procedures.

# 1 INTRODUCTION

Geologic structures (i.e., normal faults) exert two primary controls on basaltic magmatism in the Basin and Range province. First, they provide the mechanism for crustal extension, producing decompression-induced partial melting in the mantle. Second, they provide pathways for magma ascent to the surface. This report analyzes the second of these controls—namely, structural control on locations of basaltic volcanism.

In the present report, the results of a diverse suite of analyses for fault and dike interaction are summarized in order to illustrate and describe the controls on fault-dike interaction. Specifically, the geological record for fault dike interaction in the Yucca Mountain (YM) region (section 2), theoretical constraints on fault-dike interactions (section 3), analog modeling results (section 4), numerical modeling results (section 5), *in-situ* stress controls (section 6), and volcano cone alignments (section 7) are examined. These results provide the technical basis for incorporating fault and dike interaction into probability and consequence analyses of igneous activity (i.e., dike intrusion, volcanism) for the proposed repository site at YM.

The structural pathways for ascent of basaltic magma are of two types (i) new dike fractures that propagate upwards uninfluenced by pre-existing structure, and (ii) dikes that are partially controlled by pre-existing fractures or faults that behave as barriers or pathways for magma ascent. Low recurrence rate basaltic volcanic activity in the Basin and Range Province occurs where magmas are generated by decompression of fertile mantle during crustal extension (e.g., McKenzie and Bickle, 1988; Rogers et al., 1995). Ascent of this magma through the crust is enhanced by crustal structures produced by extension. This correlation between basaltic volcanism and structure occurs across a range of scales, from the superposition of individual faults and vents to the occurrence of entire volcanic fields at the margins of extensional basins (Parsons and Thompson, 1991; Conway et al., 1997). Capture of ascending basaltic dikes by faults is important for volcanic risk assessments because of the potential for lateral diversion of basalt, thereby producing intrusion or volcanic eruptions laterally offset from the location of magma generation (Connor et al., 1996). Conceivably, this lateral diversion could have beneficial or adverse consequences for a specific site by diverting magma away from or towards the site.

There are several possible modes of interaction between a vertically propagating dike (figure 1-1a) and a pre-existing planar weakness such as a fault or fracture zone. The dike may (i) propagate vertically across the fault plane (figure 1-1b); (ii) intrude the fault plane and use it as a conduit (figure 1-1c); (iii) use the fault as a pathway for some distance then break out up-dip, to propagate vertically toward the surface (figure 1-1d); (iv) bifurcate upon intersecting a fault, with the fault capturing one branch of the dike while the other branch continues to vertically propagate (figure 1-1e); or (v) terminate beneath the fault, accommodating horizontal extension by dike widening beneath the fault and fault slip above the top of the dike (figure 1-1f).

The potential for lateral diversion of magma given that capture has occurred is particularly important to the performance of the proposed high-level radioactive waste repository at Yucca Mountain, Nevada, which lies within or along the edge of the active Crater Flat volcanic field, a low-volume basaltic volcanic field (e.g., Connor and Hill, 1995). The proposed repository site is 10–15 km northeast of the center of recurrence for volcanism in the Crater Flat volcanic field. The proposed repository site, however, is within a system of west-dipping normal faults, which might be capable of channeling magma laterally away from the area of highest recurrence rates in Crater Flat volcanic field towards the repository site.

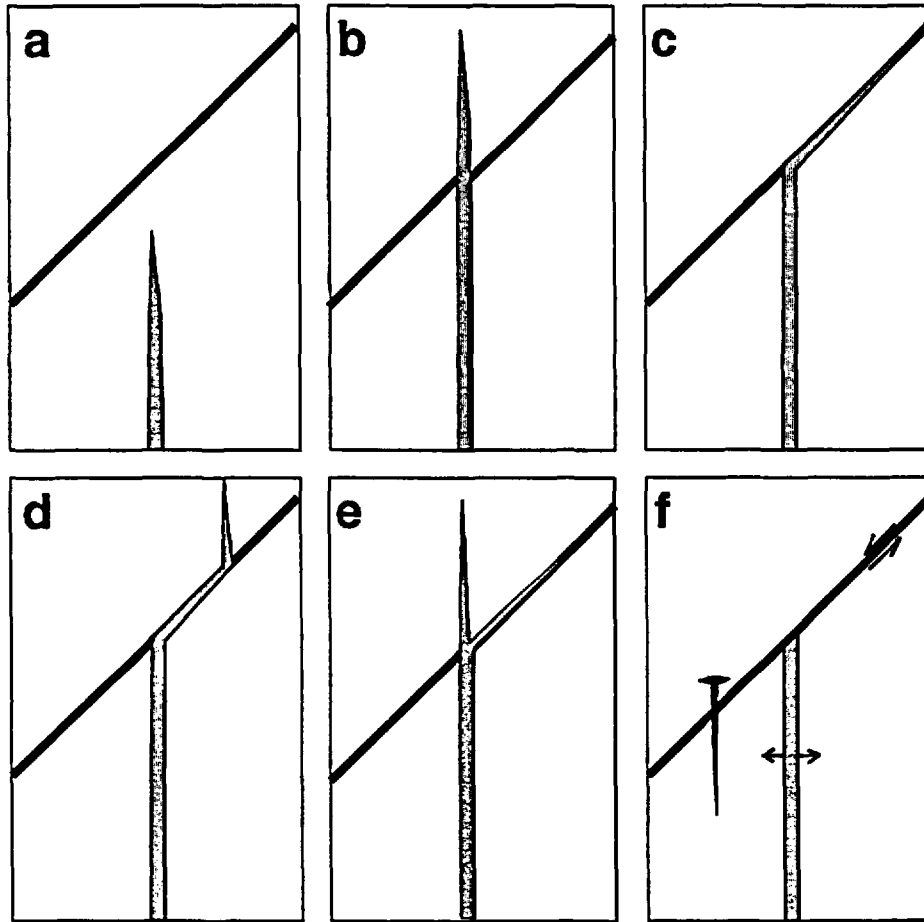


**Figure 1-1. Schematic models of fault-dike interaction in profile. Ascending magma is represented by gray pattern and faults are illustrated by thick black lines.**

The lateral distance of magma diversion ( $d$ ) once capture has occurred is a function of the dip ( $\alpha$ ) of the fault and the vertical distance of magma channeling along the fault ( $h$ ) (see figure 1-2) as defined by the equation:

$$d = h / (\tan \alpha) \quad (1-1)$$

For a dike captured by a fault, lateral diversion increases with decreasing fault dip and increasing vertical distance of magma channeling (figure 1-3).

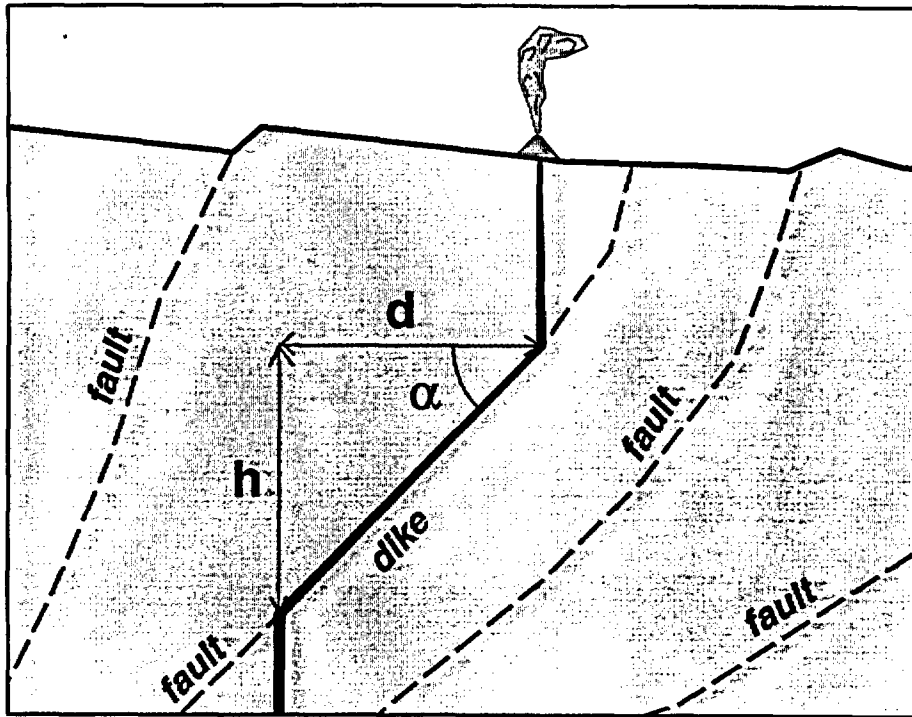


Figure 1-2. Lateral diversion distance ( $d$ ) is defined as a function of the vertical distance of dike capture by a fault ( $h$ ), and the dip of the fault ( $\alpha$ ).

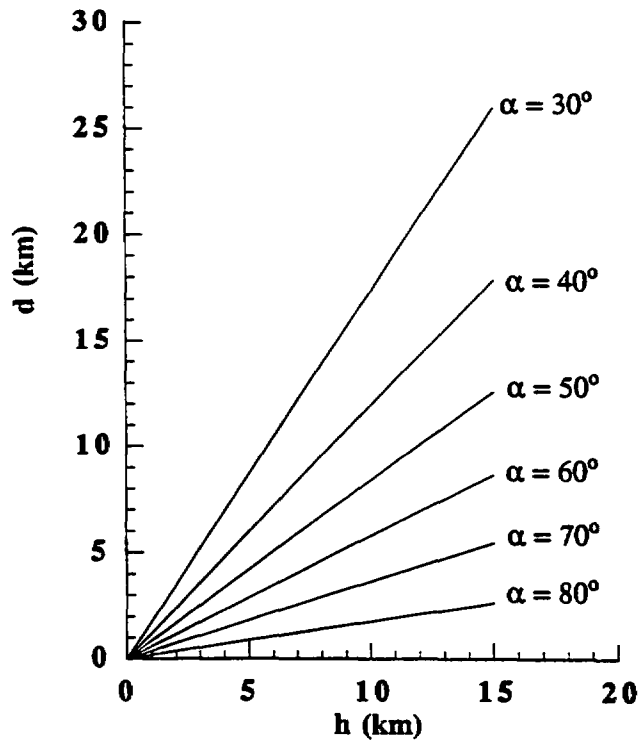


Figure 1-3. Graphical illustration of the amount of lateral diversion of a dike ( $d$ ) once dike capture has occurred given the vertical distance of dike capture ( $h$ ) and fault dip ( $\alpha$ ).

## 2 INDICATIONS OF FAULT-DIKE INTERACTION NEAR YUCCA MOUNTAIN

Observations in the YM region indicate there is a strong correlation at the local scale between geologic structures and basaltic volcanism. These observations include the development of volcanic vent alignments (Smith et al., 1990; Connor et al., 1997) and occurrence of cinder cones along faults (Connor et al., 1997). Faults and related structures likely influence magma ascent, at least on local scales, in the YM region, and this influence should be considered in volcanic hazard analyses of the proposed repository.

The strongest evidence supporting fault-channeling of dikes is the occurrence of basaltic dikes in fault zones with Miocene tuffs at YM and in the nearby Bullfrog Hills. An approximately 11 Ma basalt dike in the Solitario Canyon fault (Crowe et al., 1983; Smith et al., 1997) extends along a ~1 km segment of the fault near the northwestern edge of the proposed repository block. The fault at the surface trends north 10 east and dips 60–65° west along this part of the fault (Simonds et al., 1995). The stress field at the time of intrusion was likely dominated by the least principal stress ( $\sigma_3$ ) oriented approximately east-west (Zoback et al., 1981). The strike trend of the fault is nearly optimal for intrusion during east-west extension. At the time of dike intrusion, however, the fault may have been steeper than its present dip. Layering in the tuffs presently dips 10–12° east (Simonds et al., 1995). If this tilt was produced in association with concomitant tilting of the fault, the original (restored) dip may have been as steep as 70–77° west. Brecciation at the Solitario Canyon dike at Little Prow indicates fault slip after dike intrusion, consistent with at least a small component of fault activity after intrusion. Similarly, basaltic dikes in the Bullfrog Hills primarily intruded along pre-existing planes of weakness such as normal faults and layering (Maldonado and Hausback, 1990). Based on the observations, non-vertical faults clearly have served as pathways for magma ascent in and near YM.

Although not as definitive as observed dikes within faults, the coincidence of volcanoes with faults and linear alignments of volcanoes near YM also is consistent with an interpretation that faults may commonly provide preferential pathways for magma ascent. Two northeast-trending alignments of basaltic volcanoes parallel the trends of many active normal faults in and surrounding YM. The 11.2 km long Crater Flat alignment consists of four Quaternary volcanic centers (Stamatakis et al., 1997b). The 4.5 km long Amargosa alignment consists of three magnetic anomalies interpreted to be three basaltic volcanoes buried by alluvium (Connor et al., 1997).

Ground magnetic data surrounding the northernmost volcano in the Crater Flat alignment (i.e., Northern Cone) indicates a strong north-south structural grain beneath the Crater Flat alluvium (Connor et al., 1997), suggesting Northern Cone erupted along a north-trending normal fault. The 0.1 Ma Lathrop Wells volcano in southern YM occurs along or near the projected intersection of three normal faults. Together, coincidence of basaltic volcanoes and faults coupled with observations of dikes that have intruded faults at YM and the Bullfrog Hills strongly indicate that faults control magma ascent and therefore positions of volcanic eruptions in the YM region.

### 3 THEORETICAL CONSIDERATIONS

Propagating dike fractures, like other hydraulic fractures, typically form perpendicular to the least principal stress, because a fracture with this orientation requires the least amount of magma pressure to open (Stevens, 1911; Anderson, 1938). Because of energy considerations, favorably oriented pre-existing faults or extension fractures will serve as pathways for magma instead of the propagation of a new dike fracture. If a pre-existing fault or extension fracture has no tensile strength, the fault or fracture is likely to dilate (e.g., capture magma) if the dike fluid pressure ( $P_d$ ) exceeds the effective normal stress (result of principal stresses and pore fluid pressure  $P_f$ ) resolved on that fracture (Daneshy, 1974; Delaney et al., 1986; Reches and Fink, 1988; Jolly and Sanderson, 1997).

The likelihood of dike dilation and capture at its intersection with a cohesionless fracture or fault is controlled by (i) the stress tensor, defined by the magnitude of the maximum, intermediate, and minimum compressive stresses ( $\sigma_1$ ,  $\sigma_2$ ,  $\sigma_3$ ); (ii) orientation of the pre-existing fracture in the stress field; (iii)  $P_d$ ; (iv)  $P_f$ ; and (v) coefficient of friction across the second fracture ( $\mu$ ). If the intersected fault or fracture has a low coefficient of friction (i.e., the two faces could easily slide past one another), a crack may be arrested by transferring horizontal extension by dike-fracture dilation into fault slip (Weertman, 1980). If an active extension fracture (i.e., perpendicular to  $\sigma_3$ ) intersects a second fracture with a similar orientation, the likelihood of dilation of the second fracture is proportionally dependent on its orientation with respect to  $\sigma_3$ ; capture is more likely for fractures nearly perpendicular to  $\sigma_3$  (Warpinski and Teufel, 1987). The pressure needed to dilate a fracture thus increases as its angle relative to  $\sigma_3$  decreases.

The magnitude of differential stress is also an important factor. In a setting with low differential stress, the normal-to- $\sigma_3$  direction represents a smaller advantage in terms of driving pressure requirements over crack propagation in other directions. Hence, low differential stress allows vertically propagating magmatic dikes to be captured (redirected) by faults or fracture zones with a broader range of orientations. These qualitative relationships have been verified by extensive theoretical and experimental work on interaction between hydrofractures and pre-existing joints (e.g., Daneshy, 1974; Weertman, 1980; Abé et al., 1985; Warpinski and Teufel, 1987).

## 4 ANALYTICAL MODELING

Analytical models summarized in this section explore the interaction between faults and dikes, for constraining the conditions under which dikes will dilate faults and use them as conduits toward the surface. Based on the observations in the preceding sections, models of dike-fault interaction must address the roles of rock properties, depth, regional stress field and fault geometry. First, however, it is necessary to evaluate whether stresses at the tip of a propagating dike are sufficient to dilate a pre-existing fracture.

### 4.1 CRACK TIP CONSIDERATIONS

An analytical model of a simple elliptical dike, patterned after Pollard's (1973) model of a pressurized, two-dimensional (2D) elliptical hole in a stressed elastic solid was applied to model stresses at the dike tip (Connor et al., 1994; McDuffie et al., 1994). Results of these stress calculations indicate sufficient tensile stress occurs around the tip of a 4,000-meter-long elliptical crack to open a pre-existing fracture of nearly any orientation. In a normal-faulting stress regime defined by vertical  $\sigma_1$ , fractures with dips as shallow as a fraction of a degree intersecting the crack tip have tensile stress across them. Theoretically the crack tip could open these shallowly dipping fractures and magma could flow into them. Most of the curvature in the ellipse, representative of the crack tip, takes place over a very small region. An ellipse with an aspect ratio of 4000:1 resembles two nearly parallel lines with very tight curves connecting them at the ends. Tensile tangential stress, which can open fractures, occurs only at the tips of the ellipse. Although stress at the dike-fracture tip is great enough to open any plane of weakness, within about 1.5 mm of the fracture tip the tangential stress is compressional and thus unfavorable for fracture dilation. Thus, whether a dike continues to propagate vertically or follows a pre-existing weakness, such as a dipping fault plane, depends on additional criteria as discussed below.

### 4.2 GEOMETRIC CONSIDERATIONS

#### 4.2.1 Model Constraints

The analytical model used to calculate dike-fault interaction consists of a static, elastic approach that compares the stress state of a vertical dike propagating by fracturing rock with the stress state of a nonvertical dike that is propagating by opening a pre-existing fault plane. This model addresses the conditions under which magma ascending from depth along a vertically propagating dike is likely to be redirected by a pre-existing structure such as a fault. One criterion for the dilation of a pre-existing structure by magma is that a dike must have sufficient driving pressure to overcome the resolved normal stress across a fracture (Delaney et al., 1986). Assuming that a dike will follow a single path, then the path that is in the normal-to- $\sigma_3$  direction by definition has the smallest normal stress for magma pressure to overcome resulting in dike intrusion. Of interest here is the threshold between breaking rock in the normal-to- $\sigma_3$  direction to form a new dike fracture, versus dilating a pre-existing cohesionless fracture (e.g., fault) that is not optimally oriented.

The undeformed rock is assumed to be uniform and homogeneous. Linear-elastic brittle behavior is assumed, implying that at some tensile stress (i.e., uniaxial tensile strength  $S_0$ ) an unconfined sample of rock will fail by extension fracture. Connor et al. (1994) and McDuffie et al. (1994) assumed that pore fluid pressure in the undeformed rock is not a significant factor. Although not necessarily realistic, this assumption is unlikely to effect the result because of high dike fluid pressure which in the model appears to be sufficient to propagate a new dike fracture.

Assuming extension fracturing, the normal stress needed to open a dike fracture to some arbitrary aperture ( $\sigma_{\text{dike}}$ ), is the sum of the uniaxial tensile strength ( $S_o$ ), the normal stress, which is the resolved stress component acting normal to the plane of interest ( $\sigma_n$ , with  $\sigma_{\text{nf}}$  for fault and  $\sigma_{\text{nd}}$  for dike), and the additional normal stress required to dilate the dike fracture to some specified aperture ( $\sigma_{\text{dd}}$ ), defined by the following equation:

$$\sigma_{\text{dike}} = S_o + \sigma_{\text{nd}} + \sigma_{\text{dd}} \quad (4-1)$$

A similar expression can be derived to estimate stress necessary to separate the walls of a fault. The fault is modeled as a plane of weakness, dipping at some angle. Because the tensile strength of the fault plane may be enhanced by mineral precipitation or recrystallization, tensile strength is modeled as some fraction  $x$  of the rock tensile strength, where  $0 \leq x \leq 1$  (i.e., 0 for a fault with no tensile strength and 1 for a fault along which the tensile strength of fault equals tensile strength of host rock). If the fault plane has annealed to the extent that it has greater strength than the tensile strength of undeformed rock, it is assumed that the propagating dike will not intrude the fault plane.

The total stress ( $\sigma_{\text{fault}}$ ) needed to open a fault or fracture plane to the same aperture ( $\sigma_{\text{df}}$ ) as the dike fracture described above is:

$$\sigma_{\text{fault}} = xS_o + \sigma_{\text{nf}} + \sigma_{\text{df}} \quad (4-2)$$

In order for a dike to follow a dipping fault zone, rather than continue to propagate vertically, the following relationship must be true,

$$\sigma_{\text{fault}} \leq \sigma_{\text{dike}} \quad (4-3)$$

The dike fracture is assumed to be optimally oriented in the stress field, that is, normal to  $\sigma_3$ . Therefore  $\sigma_n$  for the vertical dike is equal to  $\sigma_3$ . In contrast, the suboptimally oriented fault has a larger resolved normal stress that must be overcome for dike intrusion to occur. This increased normal stress is affected by decreased tensile strength of the fault, so that a fault with no tensile strength may be favored over breaking a new fracture through pristine rock even though the normal stress across the fault is larger than  $\sigma_3$ .

## 4.2.2 Results

Connor et al. (1994) and McDuffie et al. (1994) studied the threshold conditions for intrusion along a fault versus new dike formation and established critical dip and depth relationships based on different rock types. Their analytical results indicate that the ability of a fault or fault zone to redirect ascending magma depends on the depth at which the fault zone is intersected and the dip of the fault zone (figure 4-1). Their calculations suggest that only high-angle faults ( $> 40-50^\circ$ ) are capable of dike capture at depths exceeding 1 km. At depths of 10 km, faults dipping at angles less than  $70^\circ$  are not likely to provide low energy pathways to the surface compared to vertical dike propagation.

Because of the relatively steep dip of faults capable of capturing and redirecting magma, lateral transport of dikes in fault zones is relatively small (see Eq. 1-1). For example, a fault dipping at  $70^\circ$  that is intersected by a dike at 10 km and bringing it all the way to the surface will result in lateral transport of  $\sim 3.6$  km. At depths less than 1 km, intermediate- to low-angle faults are also capable of capturing

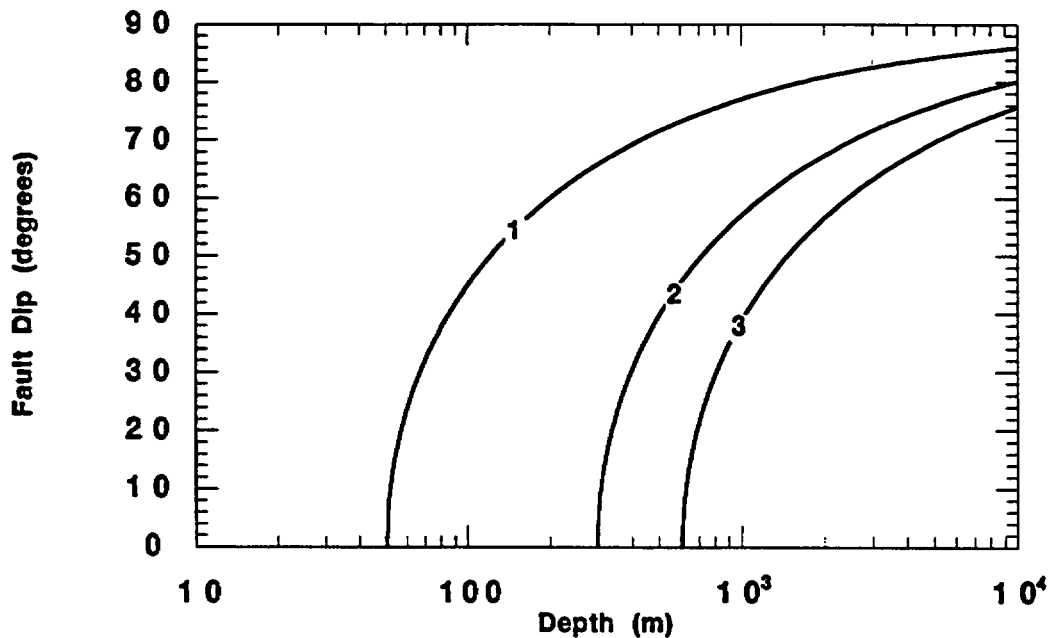


**Figure 4-1. Summary diagram from analytical modeling of fault-dike interaction (after Connor et al., 1993; McDuffie et al., 1994) illustrating theoretical thresholds between vertical dike propagation versus intrusion along the fault. Area below curves represent dip and depth values for which vertical dike propagation (figure 1-1b) is expected instead of intrusion along the fault (figure 1-1c). Area above curves (steeper or shallower depths) indicate expected fault intrusion. Curves labelled 1, 2, and 3 represent threshold values for three rock types with tensile strengths of 1, 5, and 10 MPa, densities of 2,700, 3,000, and 3,300 kg/m<sup>3</sup>, and Poisson's ratios of 0.2, 0.3, and 0.33, respectively.**

dikes. Again, however, lateral transport is rather limited; a dike intersecting a fault dipping 30° at a depth of 1 km will result in lateral offset of only 1.7 km. Thus, although unlikely, magma could be captured by a steep dike at 10 km depth and recaptured by a low-angle fault at 1 km depth. Total lateral offset of a dike captured in this extreme case yields an upper bound of 5 km of lateral diversion.

## 5 NUMERICAL MODELING RESULTS

Dynamic analysis of the interaction of a vertically propagating dike with a pre-existing fault was simulated using the DYNA3D explicit finite element code (see appendix A). Models were run to evaluate the potential for capture of a vertically propagating dike by a fault dipping at 30°, 50°, and 70° intersected at depths of 1, 2, and 5 km. The dike in each model was modeled as a magma-driven extension fracture defined using contact elements that require a threshold tensile stress to cause failure by fracture dilation. The fault in each model was simulated by two smooth surfaces with no tensile strength. Frictional resistance to sliding, however, was applied to prevent fault slip under static loading conditions.

The simulations indicate that the magma pressure ( $P_f$ ) can propagate the dike fracture by applying pressure normal to the fracture surface. The pressure required to open the vertical dike fracture is determined in part by the compressibility of the rock and in part by the overburden stress. The magnitude of the tensile strength of the rock (at least up to 20 MPa) seems to have little impact on the propagation of the dike fracture. The displacement of the dike wall is sensitive primarily to the compressibility of the host rock, the dike pressure, and the horizontal stress gradient in the host rock developed by the dike expansion.

The distance between the magma pressure head and the crack tip, called the crack tip length, decreases with increasing depth. At 1 km depth this distance is on the order of 450 m, but at 5 km depth the crack tip length is less than 50 m. When crack tip length is short, magma pressure is able to open the fault before the crack tip can progress beyond the point where the dike intersects the fault, thereby increasing the likelihood of magma intruding the fault zone. When the crack tip length is long, results of the simulations are consistent with published theoretical studies. Theoretical studies (see section 4.1) concluded that the crack tip stresses, although able to locally dilate a fault plane, were unlikely to produce intrusion along the fault because of the large distance between the crack tip and the dike pressure head (see appendix A).

Based on the calculations at 1 km and 2 km depths, the general trend is that dikes will propagate past faults with dips below a critical value, and open the faults with dips steeper than the critical dip value (figure 5-1). Based on these calculations, the critical dip value for fault-dike interaction at a depth of 1 km is near 50° and at 2 km the critical dip value is near 70° degrees. At 5 km depth, the 50° and 70° faults dilated while the simulated vertical dike fracture remained closed, but the fault openings were less than half the width of the faults opened at 1 and 2 km depth. In addition, the 5-km-deep faults narrowed to less than 0.1 m width a short distance from the dike, a width perhaps too narrow to support magma flow. Therefore, based on the dynamic analyses, 5-km-deep faults dipping at 50° and 70° are both intermediate cases between vertical dike propagation and fault intrusion. Under these circumstances, subtle variations of fault strength and rock strength may cause short-distance fault channeling rather than simple vertical dike propagation or fault capture.

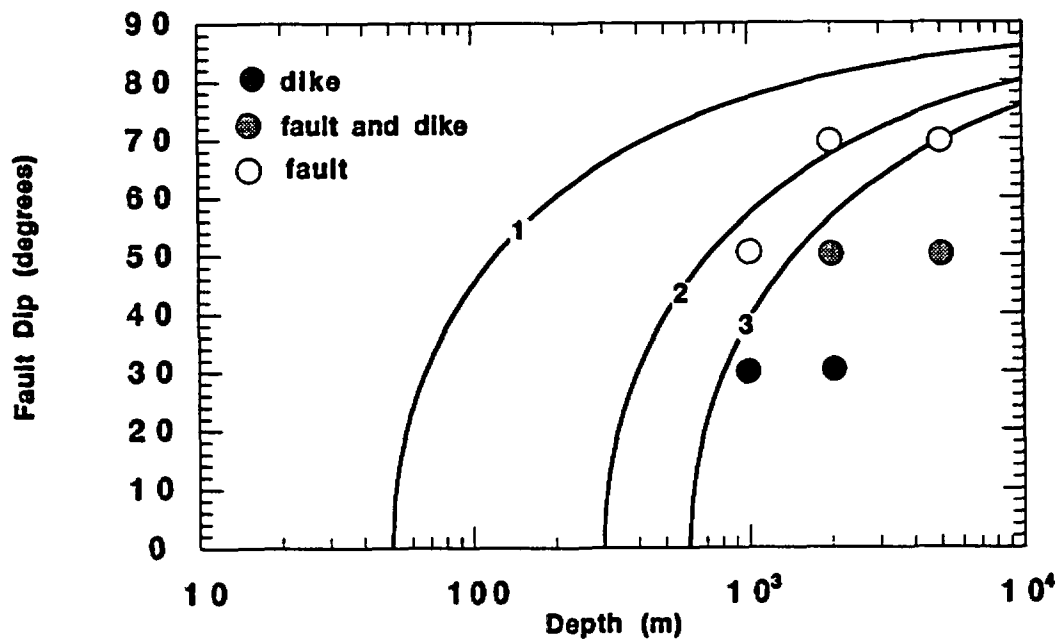


Figure 5-1. Summary diagram from analytical modeling of fault-dike interaction (figure 3) with results of numerical dynamic analyses (appendix A) illustrated using dots.

## 6 *IN SITU* STRESS AND FAULT-DIKE INTERACTION AT YUCCA MOUNTAIN

The ability of any fault or fracture to dilate during magma injection is directly related to the normal stress acting across the fracture. Assuming cohesionless faults, the relative tendency for a fault of a given orientation to dilate in a given stress state (i.e., dilation tendency), can be expressed by comparing the normal stress acting across the fault with the differential stress. Ferrill et al. (1995) define the dilation tendency of a surface as:

$$T_d = (\sigma_1 - \sigma_n) / (\sigma_1 - \sigma_3) \quad (6-1)$$

where  $\sigma_n$  is the stress normal to a fault or fracture.

Through dilation tendency analysis, the magnitude of  $\sigma_n$  is determined for surfaces of all orientations within a given stress state and then normalized by comparison with the differential stress. Thus, dilation-tendency analysis is a tool for assessing the relative potential for fracture dilation based on the resolved normal stress.

Faults with  $T_d$  greater than some threshold value, such as 0.8, are considered to have a high dilation tendency. In the YM region,  $\sigma_1$  is vertical,  $\sigma_2$  is horizontal and oriented  $028^\circ$ , and  $\sigma_3$  is horizontal and oriented  $298^\circ$ . The relative magnitudes of effective stresses (after correction for assumed hydrostatic pore fluid pressure) at a depth of 5 km are estimated to be 90:65:25 (Morris et al., 1996). As a result of this stress pattern, steeply dipping north to northeast-trending faults have a greater dilation tendency than faults of other orientations (figure 6-1). Areas with higher concentrations of high dilation-tendency faults, therefore, may be more likely to be the sites of volcanic activity. Such high dilation-tendency faults may serve as conduits for magmas ascending periodically through the crust over prolonged periods of time, resulting in the formation of cinder cone alignments (Conway et al., 1997).

A lower-hemisphere equal angle stereographic projection of dilation tendency and fault poles indicates that, in the YM region, faults trending approximately  $355-065^\circ$  with dips  $60-90^\circ$  have high dilation tendency ( $> 80$  percent of maximum  $T_d$ ; figure 6-1). Steeply dipping faults with high dilation tendency in the YM region (figure 3-3 in Stamatakos et al., 1997a) include many faults in and around the YM block, such as the Solitario Canyon fault, which bounds the repository along its western side, the Ghost Dance fault, which bisects the repository from north to south, and the Bow Ridge fault, located east of the repository site. Some of these faults, such as the Solitario Canyon fault, likely extend to detachment faults at depths of 5–12 km (Ferrill et al., 1996b). Therefore, these faults have the potential to serve as low-energy pathways for magma transport to the surface. The distribution of faults with a relatively high potential for acting as magma conduits can be inferred from geologic mapping.

Two balanced cross-sections across Bare Mountain, Crater Flat, and YM illustrate alternative interpretations of subsurface faulting at YM (figure 6-2). In the first model (Ferrill et al., 1996b; Ofoegbu and Ferrill, 1996), steep YM faults at the surface have decreasing dip with depth, and at a depth of about 6 km sole into a gently westward dipping detachment. The geometry of this model is the most reasonable for obtaining a balanced restored cross section of the upper crustal section. In the alternative model (Ofoegbu and Ferrill, 1996; Ferrill et al., 1996b), faults remain steep, or steepen with depth, until they intersect a subhorizontal detachment near the brittle-ductile transition at a depth of about 12 km.

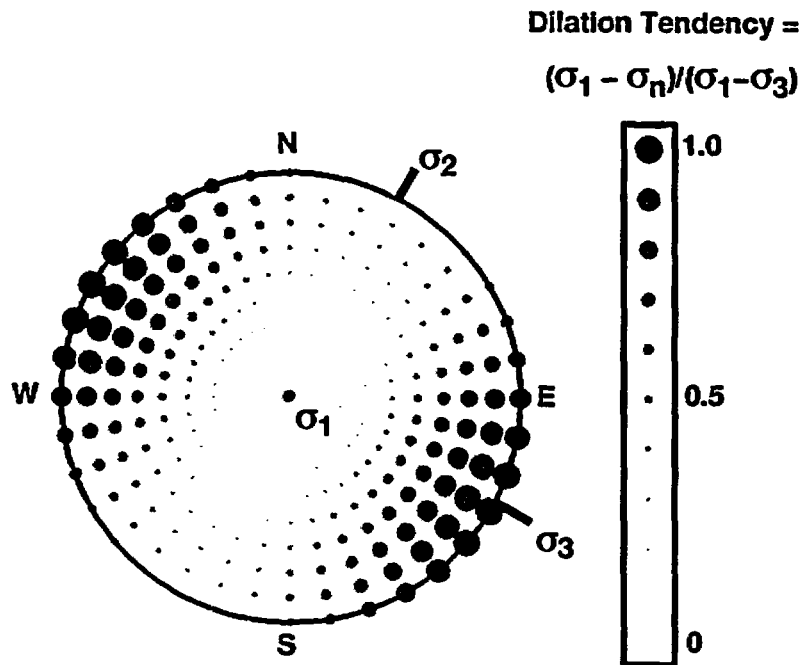


**Figure 6-1. Dilation tendency plot for the Yucca Mountain area in present day stress field (stress field from Ferrill et al., 1996b and Morris et al., 1996).**

Both shallow and moderately deep detachment models may influence basaltic magmatic activity in two ways. Steep fault segments, regardless of detachment depth, may serve as conduits for magma ascent in the shallow crust, if these faults provide relatively low-energy pathways to the surface (McDuffie et al., 1994; Jolly and Sanderson, 1997). The deep detachment model provides potentially longer pathways, and therefore potentially larger lateral distances of magma transfer from the magma source position. However, the deep detachment model also predicts steeper fault dips, thereby limiting the distance of lateral dike diversion possible by intrusion along faults.

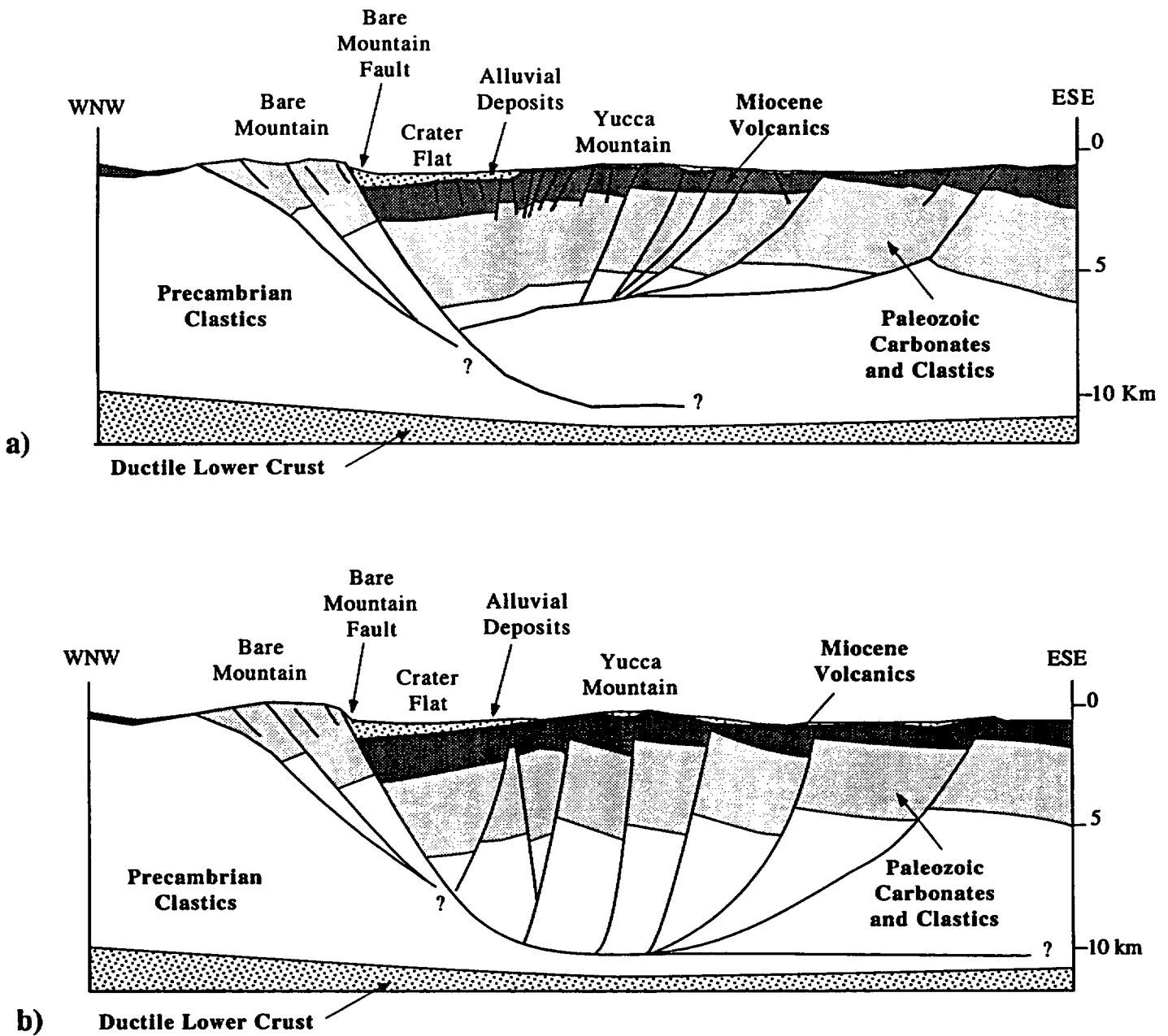


**Figure 6-2.** Cross sections through Crater Flat and Bare Mountain showing two alternative interpretations for fault geometries. a) Moderate detachment beneath Yucca Mountain in which the detachment fault links with the Bare Mountain fault at about 6 km depth. b) Deep detachment system in which all faults merge at a common detachment at about 12 km depth.

## 7 VOLCANO ALIGNMENTS

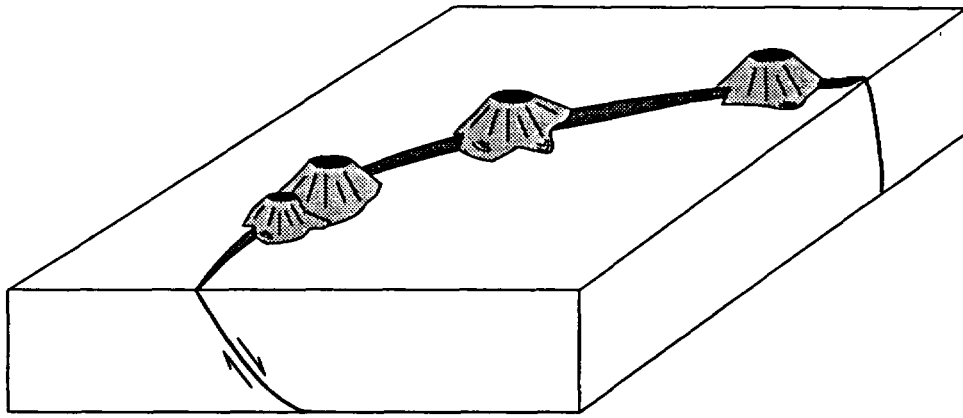
Given the theoretical, analytical, and experimental considerations of fault channeling of magma, several alternative geometric models can be developed to explain volcano alignment in the YM region (figure 7-1). These models are end-member cases and combinations of these features also are possible.

In the first model, volcano alignment is simply the result of dike capture along a steeply dipping fault with eruptions localized along the surface trace of the fault (figure 7-1a). If dikes break out from the fault at some depth controlled by near surface stresses, volcanoes will be offset into the hangingwall from the surface trace of the host fault. In the San Francisco volcanic field, numerous Quaternary basaltic cinder cones and fissure vents occur along the surface trace of the Mesa Butte fault, indicating that the fault has repeatedly served as a conduit for basaltic magma to the surface (Conway et al., 1997).

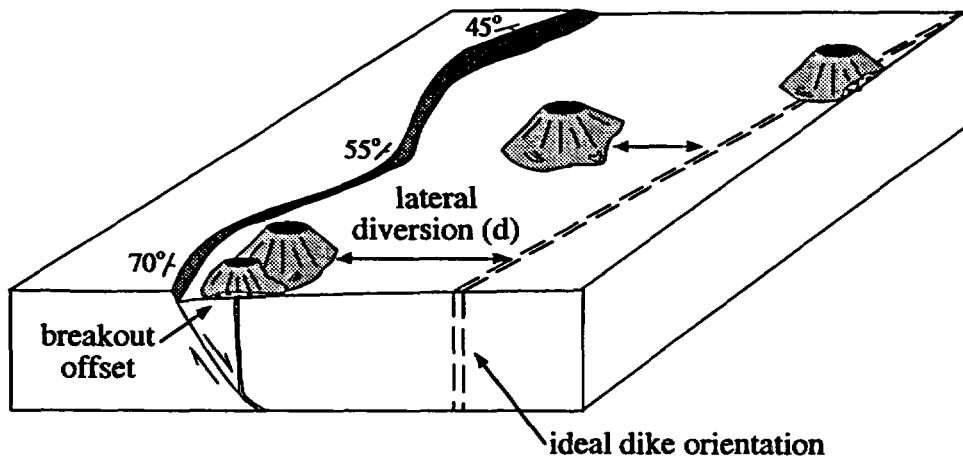
In the second model, volcano alignment results from regular lateral variations in fault dip (figure 7-1b). Volcanoes may rest atop or near the surface trace of the fault where the fault dips steeply, but volcanoes are further from the surface trace of the fault where the fault dips less steeply. Decrease in fault dip raises the resolved normal stress, thereby increasing the fluid pressure ( $P_d$ ) necessary for fault dilation, favoring ascent by vertical fracture propagation and reducing the likelihood of long-distance channeling along the fault. Breakout of the magma into the hangingwall carries the magma further away from the fault plane which can be described as breakout offset. Breakout offset may explain the volcano alignment in Crater Flat, where the alignment is not coincident with any known faults but oblique to the Bare Mountain fault. Structural (e.g., Monsen et al., 1992; Ferrill et al., 1996a) and unpublished geophysical data suggest the Bare Mountain fault changes dip from about  $45^\circ$  in northern Crater Flat near Tram Ridge to nearly  $70^\circ$  in southern Crater Flat near Steve's Pass. This lateral variation in fault dip corresponds to a southward increase in the amount of extension in the basin (e.g., Scott, 1990; Ferrill et al., 1996a; Stamatakos et al., 1997b) and may be consistent with the breakout offset model. Black Cone and Northern Cone are 6-7 km east of the northern Bare Mountain fault, where fault dip is relatively shallow (Ferrill et al., 1996a, 1997). In contrast, the two Little Cones are 2 km east of the surface trace of the Southern Bare Mountain fault, where fault dip is steepest (Ferrill et al., 1996a, 1997). Red Cone is intermediate between Black Cone and the Little Cones along a segment of the Bare Mountain fault where the dip is intermediate.

In the third model, volcano alignment arises from an *en echelon* branching array geometry (figure 7-1c). At the surface, the master fault is represented by a series of *en echelon* faults with orientations oblique to the overall strike of the master fault dike at depth. Volcano alignments may form along one or more of the *en echelon* branches and therefore, oblique to the trend of the master fault at depth. This *en echelon* relationship, for example, could explain the relationship of the prominent north trending local structures at Northern Cone, defined by ground magnetic surveying (Connor et al., 1997), to the overall northeast trend of the Crater Flat volcano alignment.

a) Cones aligned along fault trace



b) Cones offset from fault with lateral variation in fault dip



c) Cones along an *en echelon* array

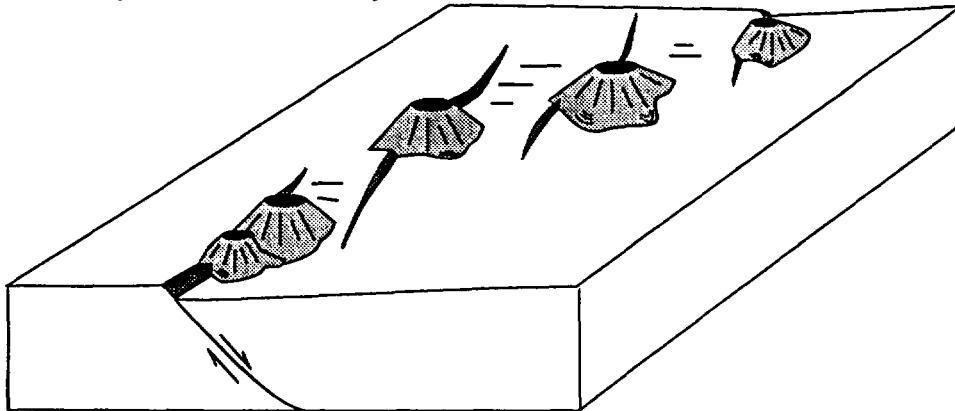


Figure 7-1. Conceptual block diagrams of potential structural control on volcanism

## 8 CONCLUSIONS

Analyses of fault-magma interactions based on geological considerations, theoretical and analog modeling results, *in-situ* stress, and three-dimensional (3D) geometric constraints suggest the following six conclusions.

- Intrusion of dikes along faults, coincidence of basaltic volcanoes with surface positions of faults, and alignments of basaltic volcanoes parallel to trends of major faults suggest that fault channeling of magma may have occurred in the YM region. Most prominently, a 60–65°-dipping segment of the Solitario Canyon fault at Little Prow was intruded by a basaltic dike at about 11 Ma, in marked similarity to intrusion of basaltic dikes along moderately dipping faults in volcanic tuffs of the Bullfrog Hills. These occurrences indicate a strong tendency for dike channeling along non-vertical faults in and around YM.
- The distance of lateral diversion of basaltic dikes by magma channeling along faults depends on the dip of the fault and depth range of magma channeling along the fault. Gentler dips and greater vertical distances of magma channeling lead to larger lateral diversions. The likelihood of magma channeling along a fault, however, decreases with decreasing fault dip.
- Analytical models indicate that at shallow depths (e.g., <0.1 to 1 km), moderate to low angle faults may be able to capture dikes. The depth of crossover between vertical dike propagation and dike capture depends on the strength of the host rock, with increasing rock tensile strength favoring dike capture by faults versus vertical dike propagation.
- Numerical modeling generally supports results of analytical modeling, however, intermediate cases were produced numerically in which the dike both intruded the 50–70° fault, and continued to propagate vertically.
- Dilation-tendency analysis incorporates fundamental relationships and produces an approach for modeling lateral or 3D variations in structural geometry, unlike 2D analytical and numerical solutions. Dilation-tendency analysis of YM faults indicates that several faults in and around the proposed repository block are in high-dilation-tendency orientations and thus are nearly optimally oriented for dike capture. These high dilation tendency faults include the Solitario Canyon fault, the Ghost Dance fault, and the Bow Ridge fault.
- Total lateral diversion of a dike captured initially by a high-angle fault and then recaptured by a low-angle fault should be no more than 3–5 km. Lateral diversion by a 60–65°-dipping fault (e.g., Solitario Canyon Fault) through 12 km of brittle crust would not exceed 6–7 km.

## 9 REFERENCES

- Abé, H., K. Hayashi, and D. Arima. 1985. Theoretical study on the stability of a reservoir created by the intersection of a fluid-filled crack with an oblique joint for the extraction of geothermal heat. *International Journal for Numerical and Analytical methods in Geomechanics* 9: 15–27.
- Anderson, E.M. 1938. The dynamics of sheet intrusion. *Proceedings of the Royal Society of Edinburgh* 58: 242–251.
- Conway, F.M., D.A. Ferrill, C.M. Hall, A.P. Morris, J.A. Stamatakos, C.B. Connor, A.N. Halliday, and C. Condit. 1997. Timing of basaltic volcanism along the Mesa Butte Fault in the San Francisco volcanic field, Arizona from  $^{40}\text{Ar}/^{39}\text{Ar}$  ages: Implications for longevity of cinder cone alignments. *Journal of Geophysical Research* 102: 815–824.
- Connor, C.B., and B.E. Hill. 1995. Three nonhomogeneous Poisson models for the probability of basaltic volcanism: Application to the Yucca Mountain region, Nevada. *Journal of Geophysical Research* 100: 10,107–10,125.
- Connor, C.B., B.E. Hill, K.H. Spivey, and P. Hunka. 1993. Volcanism Research. *NRC High-Level Radioactive Waste Research at CNWRA, July-December 1993.10-1-10-26*. B. Sagar, ed. San Antonio, Texas: Center for Nuclear Waste Regulatory Analyses: 121–139.
- Connor, C.B., S. Lane-Magsino, J.A. Stamatakos, R.H. Martin, P.C. La Femina, B.E. Hill, and S. Lieber. 1997. Magnetic surveys help reassess volcanic hazards at Yucca Mountain, Nevada. *EOS, Transactions, American Geophysical Union* 78: 73 77–78.
- Connor, C.B., S. McDuffie, and B.E. Hill. 1994. Field volcanism research. *NRC High-Level Radioactive Waste Research at CNWRA, July-December 1993*. B. Sagar, ed. San Antonio, Texas: Center for Nuclear Waste Regulatory Analyses: 10–1 to 10–26.
- Connor, C.B., J.A. Stamatakos, D.A. Ferrill, and B.E. Hill. 1996. Integrating structural models into probabilistic volcanic hazard analyses: An example from Yucca Mountain, NV. *Geological Society of America, 1996 Annual Meeting, Abstracts with Programs, October 28-31, 1996*. Denver, CO: Geological Society of America: A-192.
- Crowe, B.M., D.T. Vaniman, and W.J. Carr. 1983. *Status of Volcanic Hazard Studies for the Nevada Nuclear Waste Storage Investigations*. Los Alamos National Laboratory Report LA-9325-MS. Los Alamos, NM: Los Alamos National Laboratory.
- Daneshy, S.S. 1974. *Hydraulic Fracture Propagation in the Presence of Planes of Weakness*. Society of Petroleum Engineers Paper Number 4852. Amsterdam, The Netherlands: Society of Petroleum Engineers.
- Delaney, P.T., D.D. Pollard, J.I. Ziony, and E.H. McKee. 1986. Field relations between dikes and joints: Emplacement processes and paleostress analysis. *Journal of Geophysical Research* 91B: 4,920–4,938.

- Ferrill, D.A., A.P. Morris, D.B. Henderson, and R.H. Martin. 1995. Tectonic processes in the central Basin and Range region. *NRC High-Level Radioactive Waste Research at CNWRA, July-December 1994*. B. Sagar, ed. San Antonio, Texas: Center for Nuclear Waste Regulatory Analyses: 121-139.
- Ferrill, D.A., J.A. Stamatakos, S.M. Jones, B. Rahe, H.L. McKague, R.H. Martin, and A.P. Morris. 1996a. Quaternary slip history of the Bare Mountain Fault (Nevada) from the morphology and distribution of alluvial fan deposits. *Geology* 24: 559-562.
- Ferrill, D.A., J.A. Stamatakos, and H.L. McKague 1997. Quaternary slip history of the Bare Mountain Fault (Nevada) from the morphology and distribution of alluvial fan deposits: Reply. *Geology* 25: 190.
- Ferrill, D.A., G.L. Stirewalt, D.B. Henderson, J.A. Stamatakos, A.P. Morris, B.P. Wernicke, and K.H. Spivey. 1996b. *Faulting in the Yucca Mountain Region: Critical Review and Analyses of Tectonic Data from the Central Basin and Range*. NUREG/CR-6401. Nuclear Regulatory Commission.
- Jolly, R.J.H., and D.L. Sanderson. 1997. A Mohr circle construction for the opening of a pre-existing fracture. *Journal of Structural Geology* 19: 887-892.
- Maldonado, F., and B.P. Hausback. 1990. *Geologic Map of the Northeast Quarter of the Bullfrog 15-Minute Quadrangle, Nye County, Nevada*. U.S. Geological Survey Miscellaneous Investigations Map I-2049. Reston, VA: U.S. Geological Survey.
- McDuffie, S.M., C.B. Connor, and K.D. Mahrer. 1994. A simple 2-D stress model of dike-fracture interaction. *EOS, Transactions of the American Geophysical Union* 75(16): 345.
- McKenzie, D., and M.J. Bickle. 1988. The volume and composition of melt generated by extension of the lithosphere. *Journal of Petrology* 29: 625-679.
- Monsen, S.A., M.D. Carr, M.C. Reheis, and P.A. Orkild. 1992. *Geologic Map of Bare Mountain, Nye County, Nevada*. U.S. Geological Survey Miscellaneous Investigations Series, Map I-2201, scale 1:24 000.
- Morris, A.P., D.A. Ferrill, and D.B. Henderson. 1996. Slip tendency analysis and fault reactivation. *Geology* 24: 275-278.
- Ofoegbu, G.I., and D.A. Ferrill. 1996. Mechanical analyses of a Yucca Mountain fault model. *Proceedings of the Topical Meeting on Methods of Seismic Hazards Evaluation, Focus '95*. American Nuclear Society: 115-124.
- Parsons, T., and G.A. Thompson. 1991. The role of magma overpressure in suppressing earthquakes and topography: Worldwide examples. *Science* 253: 1,399-1,402.
- Pollard, D.D. 1973. Equations for stress and displacement fields around pressurized elliptical holes in elastic solids. *Mathematical Geology* 5: 11-25.

- Reches, Z., and K. Fink. 1988. The mechanism of the intrusion of the Inyo Dike, Long Valley Caldera, California. *Journal of Geophysical Research* 93B: 4,321–4,334.
- Rogers, N.W., C.J. Hawkesworth, and D.S. Ormerod. 1995. Late Cenozoic basaltic magmatism in the Western Great Basin, California and Nevada. *Journal of Geophysical Research* 100(B7): 10,287–10,301.
- Scott, R.B. 1990. Tectonic setting of Yucca Mountain, southwest Nevada. Basin and Range extensional tectonics near the latitude of Las Vegas, Nevada. B.P. Wernicke, ed. *Geological Society of America Memoir* 176: 251–282.
- Simonds, F.W., J.W. Whitney, K.F. Fox, A.R. Ramelli, J.C. Yount, M.D. Carr, C.M. Menges, R.P. Dickerson, and R.B. Scott. 1995. Map showing fault activity in the Yucca Mountain area, Nye County, Nevada. U.S. Geological Survey Miscellaneous Investigations Series Map I-2520: Scale 1:24,000.
- Smith, E.I., D.L. Feuerbach, T.R. Naumann, and J.E. Faulds. 1990. The area of most recent volcanism near Yucca Mountain, Nevada: Implications for volcanic risk assessment. *High-Level Radioactive Waste Management: Proceedings of the First Annual International Conference, La Grange, Illinois*. American Nuclear Society 1: 81–90.
- Smith, E.I., S. Morikawa, and A. Sanchez. 1997. *Summary of the Activities of the Center for Volcanic and Tectonic Studies, University of Nevada, Las Vegas, for the Period 1986–1996*. Carson City, Nevada: The Nuclear Waste Project Office.
- Stamatakos, J.A., C.B. Connor, and R.H. Martin. 1997b. Quaternary basin evolution and basaltic volcanisms of Crater Flat, Nevada, from detailed ground magnetic surveys of the Little Cones. *Journal of Geology* 105: 319–330.
- Stamatakos, J.A., P.S. Justus, D.A. Ferrill, R. Chen, and G.I. Ofoegbu. 1997a. Structural Deformation and Seismicity. *NRC High-Level Radioactive Waste Program Annual Progress Report: Fiscal year 1996*. B. Sagar, ed. NUREG/CR-6513, No. 1, CNWRA 96-OIA. San Antonio, TX: Center for Nuclear Waste Regulatory Analyses.
- Stevens, B. 1911. The laws of intrusion. *Transactions of the American Institute of Mining Engineers* 41: 650–672.
- Warpinski, N.R., and L.W. Teufel. 1987. Influence of geologic discontinuities on hydraulic fracture propagation. *Journal of Petroleum Technology* 39: 209–220.
- Weertman, J. 1980. The stopping of a rising, liquid-filled crack in the earth's crust by a freely slipping horizontal joint. *Journal of Geophysical Research* 85B: 967–976.
- Zoback, M.L., R.E. Anderson, and G.A. Thompson. 1981. Cainozoic evolution of the state of stress and style of tectonism of the Basin and Range Province of the western United States. *Philosophical Transactions of the Royal Society of London* A300: 407–434.

## **APPENDIX**

# **SIMULATION OF DIKE PROPAGATION AND DEFLECTION BY A FAULT**

*Prepared by*

**Robert W. Terhune  
Integrated Parallel Technology, Inc.  
1181 Quarry Lane Blvd 400, Suite A  
Pleasanton, CA 94566**

A-1

9710240156 970918  
PDR WASTE PDR  
WM-11

# 1 SUMMARY

Computer simulations of dike fracture extension in an elastic media were made to evaluate the hypothesis that an intersecting fault may redirect an upwardly propagating dike. The key parameters of the study are the depth of intersection of the dike with the fault and the fault dip angle. The simulations indicate that the magma can propagate the dike fracture by applying pressure normal to the fracture surface. The pressure required to open the dike fracture is determined in part by the compressibility of the rock and in part by the overburden stress. The magnitude of the tensile strength of the rock (at least up to 0.02 GPa) seems to have little influence on the propagation of the dike fracture. The displacement of the dike wall is sensitive primarily to the compressibility of the host rock, the dike pressure, and the horizontal stress gradient in the host rock developed by the dike expansion. The distance between the pressure head and the crack tip, called the crack tip length, decreases with depth. At 1 km depth this distance is on the order of 450 m while at 5 km depth the crack tip length is less than 50 m. When the crack tip length is short, the dike pressure is able to open the fault before the crack tip can progress beyond the point where the dike intersects the fault. When the crack tip length is long, the results of the simulations are consistent with published theoretical studies. Based on the calculations at 1 km and 2 km depth, the general trend is that the dike will propagate past faults below a critical dip value, where the fault remains closed, and opens the faults with dips above the critical dip value, where the dike remains closed. Based on the calculations the critical dip value for 1 km is near 50 degrees and for 2 km the critical dip value is near 70 degrees. At 5 km depth, the faults at dips of 50 and 70 degrees opened up while the dike remained closed, but the fault openings were less than half the width of the open faults at 1 and 2 km depth. In addition, the faults narrowed to less than 0.1 m width a short distance from the dike and are unlikely to support magma flow. The pressure that is required to propagate the magma is about half the overburden pressure at 5 km, which would be insufficient to further open a dipping fault. Consequently, at depths on the order of 5 km, it is hypothesized that the fault would open slightly, but would not propagate to any great distance. Thus vertical magma ascent would continue when faults dipping 70° or less were encountered at 5 km.

## 2 INTRODUCTION

### 2.1 HYPOTHESIS TO BE EVALUATED

It is assumed that for a propagating dike that intersects a fault, there is some dip angle of the fault for a given fault-dike intersection depth that the magma will move up the fault instead of continuing to propagate the dike fracture.

### 2.2 SCOPE OF WORK

Based on the work of Connor et al. (1994), which calculated the minimum dip angle of a fault that would redirect the magma of an upwardly propagating dike, figure 1 shows the curves for tensile strength of 0.005 GPa. ( $h_0 = 50.4$  m) and 0.01 GPa ( $h_0 = 609$  m). The material properties used for figure 1 were density 3.3 Mg/m<sup>3</sup>, Poisson's ratio of 0.33 and tensile strength of 0.01 GPa. In comparison the proposed simulations used a density of 2.7 Mg/m<sup>3</sup>, Poisson's ratio of 0.25 and tensile strength of 0.01 GPa to give a  $h_0 = 588$ . The difference between the parameters of this study and Connor et al. (1994) if plotted on figure 1 would be approximately the thickness of one of the curves.

Using the computer code DYNA3D, the simulation of a propagating dike where the path of the dike crosses a fault was modeled. This report is the result of a parameter study where the parameters of the study are the depth of the intersection and the dip of the fault as given below.

Depths	1, 2, and 5 km
Dips	30°, 50°, and 70°

It is desirable that some of the calculations model the entire region between the intersection and the surface. The depths and dip angles for the calculations were selected to examine the regions bounded by the  $h_0 = 609$  m curve in figure 1.

### 2.3 METHOD OF ANALYSIS

The method of analysis is to simulate the pressure created by the magma in a dike, modeling the tensile fracturing of the rock, the opening of the dike, and growth of the dike tip using the computer code DYNA3D. The dike is modeled as two surfaces bonded together with bonds having a tensile strength of 0.01 GPa. The intersecting fault is modeled as two smooth surfaces with frictional sliding forces to resist motion on the fault. The coefficient of friction specified was 1.2 which is equal to the tangent of 50 degrees. The tensile strength across the fault surfaces is zero.

#### 2.3.1 DYNA3D Computer Model

##### 2.3.1.1 Units

DYNA3D will accept any set of consistent units. The following units were used for this study.

Parameter	Units	Abbreviation
Distance	meters	m
Time	milliseconds	ms
Mass	Megagrams	Mg
Force	Giga-Newton	GN
Stress	Giga-Pascal	GPa
Energy	Giga-Joules	GJ
Energy	Giga-Joules	GJ
Density	Mg/m <sup>3</sup>	
Velocity	m/ms	
Acceleration	m/(ms) <sup>2</sup>	

### 2.3.2 DYNA3D Description

DYNA3D (Whirley and Hallquist, 1991) is a explicit finite element code for analyzing the transient dynamic response of three dimensional solids and structures. The code is developed and maintained by the Methods Development Group, Mechanical Engineering Department, of the Lawrence Livermore National Laboratory, Livermore, California.

The basic unit for modeling solids in the DYNA3D computer code is the 8 node continuum element. The elements used in this study are primarily rectangular brick shapes. Forces applied to the nodes, stress the element, the behavior of which is determined by the material model designated for the element. A set of "n by m" elements form a block where n and m are integers. All elements of a block have the same material properties and a common set of external boundaries. The nodes of the elements carry global location, displacement, velocity, and acceleration. The elements carry the stresses and strains. The global model can consist of one or more blocks plus initial conditions, and global boundary conditions.

Global models consisting of more than one block, must have the blocks connected to each other such that the stresses and displacements are transmitted between blocks. The blocks are tied together by slip surfaces that link each node of one block's boundary surface to the boundary surface of an adjacent block and visa versa. The DYNA3D code has approximately 10 different types of slip surfaces of which only three are of concern for this study. These are:

- Tied slip to lock two blocks together. Stresses, strains, displacements and stress waves will transmit across a tied slip as though the blocks were one. The tied slip is useful for joining blocks of different shapes, different element size (zoning), or different materials.
- Sliding with separation and friction. This type of slip is useful where the model calls for frictional slippage and separation of two parts of the model such as the fault. Both the static and kinetic coefficient of friction are defined as well as the time constant required to adjust from static to kinetic conditions. For this study, motion along the fault is assumed to be approximated by the static condition.
- Tied slip with failure. This type of slip is useful where the model calls for separation of the blocks due to failure of the matrix material such as the dike fracture. The bonds that tie the nodes of one block to the surface of another have both a tensile strength and shear strength defined that must be exceeded before the blocks can slip or separate from each other. In addition, if slippage occurs under shear stresses then frictional forces apply as above. Note that the path of the fracture is defined by the surface of the blocks. This is referred as break-slip later in the text.

The boundaries of a block can also accept a time history of stress, which for this effort is used to simulate the magma pressure and the propagation of the magma up the dike. Global boundaries are defined by restraining the displacement of the block surface nodes in the direction normal to the surface. The free surface is modeled for all of the 1 km and 2 km calculations and some of the 5 km calculations.

### 2.3.2.1 Assumptions

A plane strain model was assumed for these calculations. Pollard (1987) describes the geometry of a generalized dike based on numerous studies as being on the order of a few meters thick, several kilometers in outcrop length, and several kilometers in depth. The displacement of the dike wall is normal to the orientation of the fracture. Consequently, it seemed a reasonable approximation to model the dike as a mode 1 blade fracture in plane strain. Creating a 3D model that would give results different from a plane strain model requires modeling significant variation of the crack geometry in the plane of the dike. Such variation is speculative and would not contribute to the primary goals of this study.

### 2.3.2.2 Overburden Stress

There is no convincing data to select one model of overburden stress over another. Under varying strain conditions within the earth, the horizontal stress may be less than, equal to, or greater than the vertical stress. The simplest model is the hydrostatic model where the horizontal stresses are equal to the vertical stress. DYNA3D has a version of this model where the vertical stress at a given point is computed from the gravity constant times the integrated density from the surface to the point at depth. Unfortunately, this method does not model the gravity body force and is not a suitable approach for this problem. To model gravity, the entire model and its coordinate system must be accelerated upward at  $980.7 \text{ cm/s}^2$ . The calculation must then go through a stress relaxation process until the stress state reaches equilibrium. This may take between 2,000 to 10,000 pseudo time cycles depending on the vertical stress, which is given by the density times the gravity constant times the depth. The horizontal stress is less than the vertical stress, being determined by Poisson's ratio.

### **2.3.2.3 External Boundary Conditions**

The boundaries were chosen to be 2,500 m horizontally distant from the dike. It is assumed that the restraining boundaries in the horizontal direction are far enough from the dike that they would have little influence on the displacement of the dike wall. Calculations showed this assumption to be true.

### **2.3.3 Geometry of Model**

The dike lies in the "y,z" plane at "x = 0" with the magma pressure applied in the horizontal "x" direction. The "y" coordinate is vertical and the gravity body force is in the negative "y" direction. The surface is at "y = 0." The vertical height of the grid is 2,500 m for all calculations at 1 km, 3,500 m for all the calculations at 2 km and 6500 m for the calculations at 5 km intersection depth. The horizontal width of all grids is 5,000 m. Except for the fault extension region the grid is close to being symmetrical about the dike plane. The "x,z" plane at "z = 0" is a plane of symmetry while a fixed boundary is at "z = -8 m". The pressurized region of the dike is the lower 1,500 m of the grid.

### **2.3.4 Zone Size**

The grid for the calculations was fine zoned for 500 m vertically above and below the intersection along the dike and 200 m on each side of the dike. By "fine" zone size we mean 20 m × 20 m. Beyond 400 m vertically, the zones increased geometrically by 5 percent to the surface and lower boundary while the horizontal zone size remained 20 m. In the horizontal direction, a zone size discontinuity was created at 200 m, where the zone size changed from 20 × 20 m to 30 × 30 m for the 1 km depth, 40 × 40 for the 2 km depth and 50 × 50 for the 5 km depth.

The primary cause of reflected waves back into the dike region is an impedance mismatch between the fine zoned region and the course zone regions at 200 m horizontal. Experiments showed that the mass of a zone was more important than the change in zone size in the direction of the wave propagation. Elimination of the reflections required an increase in the zone mass of less than 5 percent.

## **2.4 MODELING DIKE PATH AND FAULT**

Some coarse zoned calculations demonstrated that the final results were the same whether the magma was propagated into the region of the intersection or if the dike was opened up below the intersection by a constant pressure. Since propagation of the magma required the calculation to run for several weeks or more, a decision was made to obtain the shorter calculation times associated with simulating simple dike openings.

The dike is modeled in two sections. The first is a section of the dike that runs from the bottom of the grid to the intersection of the fault. The second section runs from the intersection point to the top of the grid. The first section is a break slip with the tensile strength set to zero. The dike crack is assumed to be formed and pressurized, which opens the dike. The second section is a break slip with the tensile strength set to 0.01 GPa. No magma pressure is applied to this section. On the first section the dike pressure is ramped up from zero at a rate of 0.01 GPa per second or less. Figure 2 compares the dike pressure required to open the dike 1.0 meter total width with the overburden pressure along the first section of the dike. The plot clearly shows that a portion of the pressure (0.2 GPa) is used against the elasticity of the rock, and a portion is used to expand against horizontal stress. The dike pressure

increases with depth at  $0.9 \times 10^{-5}$  GPa/m, which is equal to the horizontal stress gradient ( $\frac{1}{3}$  of overburden gradient of  $2.65 \times 10^{-5}$  GPa/m).

The fault is modeled as two adjoining smooth surfaces with a coefficient of friction equal to the tangent of  $50^\circ$ . The fault in the down dip direction ran to 200 m horizontally in all cases. The fault in the up dip direction ran to 1000 m horizontally for the  $30^\circ$  dip, 600 m horizontally for the  $50^\circ$  dip, and 400 m horizontally for the  $70^\circ$  dip.

## 2.5 MEDIUM PARAMETERS

### 2.5.1 Rock Properties

Based on the low stresses involved the host rock was modeled as a purely elastic media with the following parameters.

Density	2.7 Mg/m <sup>3</sup>
Poisson's ratio	0.25
Young's modulus	48.7 GPa
Bulk modulus	32.5 GPa
Shear modulus	19.5 GPa
Dike tensile strength	0.01 GPa
Fault friction angle	$50^\circ$ (Tan $50^\circ = 1.2$ )

### 2.5.2 Dike Shape as a Function Depth

A series of calculations was done where only the dike was modeled, and divided into two sections, one pressurized and the other unpressurized and bonded with bonds of 0.01 GPa of tensile strength. The displacement along the dike wall of the pressurized region was fairly constant between 500 and 1,000 m below the pressure head. Below 1,000 m the dike wall displacement was reduced by the increased overburden pressure. Based on this we modeled the pressurized region of the dike to a depth of 1,500 m below the pressure head for a given dike pressure. A series of calculations was run to determine the dike pressure required to displace the dike walls 0.5 m to give a total dike width of 1 m. The results of this study are shown in figure 2. The pressure required to open the dike is a function of both the compressibility of the rock and the overburden pressure. The overburden pressure points in figure 2 give the pressure range from the given depth to 1,500 m below the given depth. The actual dike pressure needed to open the dike is equal to the overburden pressure at 1 km but increases much less than the overburden with an increase in depth.

The crack shape between 500 m above the pressure head and 500 m below the pressure head is shown in figure 3, for four depths. The depth shown was normalized by subtracting the depth where

the pressure was applied from the depth of the data point. Note that the crack shape at 1 km is considerably different from the shape at other depths.

Two conclusions were made based on this parameter study

- The crack tip grows beyond the pressurized region and the crack shape is similar to the cohesive zone model defined by Pollard (1987) and shown in figure 4.
- The distance above the pressure head to which the crack tip grows is dependent on the depth of the applied pressure head. This distance from the end of the pressurized zone to the crack tip is shown in figure 4 as "L." Figure 5 shows a plot of the crack tip length "L" as a function of depth. At 650 m depth the crack would extend to the surface and at 5 km depth "L" is approximately 50 m.

## **2.6 Dike-Fault Interaction Studies**

The logic for the order of the dike-fault calculations was as follows: Start with depth 1 km, dip 30°. If the dike propagates and the fault remains closed, do the next larger dip for the same depth. If the dike does not propagate and the fault opens, then do the same dip at the next depth. If both open, do the next dip at the same depth and the previous dip at the same depth. The order of presentation is with respect to increasing depth and increasing dip.

### **2.6.1 Results for Depth 1 km, Dip 30°**

The dike opened a total width of 0.52 m at the intersection point and a maximum of approximately 1 m at depth. Figure 6 shows the grid with horizontal displacement contours after maximum dike wall displacement. The horizontal displacement has been magnified by a factor of 20 to better show the dike opening. The fault here appears tightly closed. At 800 m the displacement contours show the dike half width is 0.11 m. The contours also show that the dike wall displacement is symmetric about the dike plane at  $x = 0$ . Figure 7 shows the displacement along the dike as a function of depth. A small indentation at the fault intersection can be seen in the upper curve. Figure 8 compares the upper 1,000 m of dike wall displacement for the dike only calculation with the dike-fault calculations. This shows that the dike-fault dike displacement behaved essentially as if the fault was absent. Figure 9 shows the fault displacement normal to the dip for both the top and bottom surface of the fault. The appearance that the fault is very slightly open is more likely due to the combined coarseness of the grid and the contour algorithm than actual displacement normal to the dip. The magma would bypass the fault and continue to propagate the dike upward.

### **2.6.2 Results for Depth 1 km, Dip 50°**

The grid spacing and initial conditions for these calculations was identical to the previous calculations. Figure 10 shows the grid with contours of the x displacement at the end of the dike expansion. The horizontal displacement has been magnified by a factor of 20 to better show the dike opening. The dike above the intersection with the fault remained unfractured and closed. The fault can be seen as clearly open up to a horizontal distance greater than 200 m. The displacement contours show the dike displacement below the intersection is symmetric. Above the intersection, both sides of the dike path moved in the negative direction. Figure 11 shows the dike displacement as a function of depth. Note

how both sides of the dike above the intersection follow the expected path of the left hand side of the dike if it was open. Again the apparent open dike above the intersection is due to the zoning and the contour algorithm. The tension bonds remained unbroken. Figure 12 compares the half-width displacement of the dike only calculation with the dike-fault calculation. Below the intersection, the dike behaves as if the fault was absent. Apparently most of the fault opening is due to horizontal displacement to the left of the section above the fault. Figure 13 shows the displacement of the fault surfaces normal to the dip angle. The maximum displacement along the fault is approximately 0.4 m. At 200 m horizontal distance the fault opening is 0.2 m. The magma would be deflected by the fault and move up the fault.

### **2.6.3 Results for Depth 2 km, Dip 30°**

Figure 14 shows the grid with horizontal displacement contours after maximum dike wall displacement. The horizontal displacement has been magnified by a factor of 20 to better show the dike opening. The fault here appears tightly closed. At 1,900 m depth the displacement contours show the dike half width is 0.12 m. The contours also show that the dike wall displacement is close to but not quite symmetric about the dike plane at  $x = 0$ . Figure 15 shows the displacement along the dike as a function of depth. The dike opened a total of 0.40 m at the intersection point (2,000 m) and a maximum of approximately 1.1 m at depth. Figure 16 compares the upper 1,000 m of dike wall half-width displacement for the dike only calculation with the dike-fault calculations. This shows that the dike-fault dike displacement behaved essentially as if the fault was absent. The displacement within the pressurized region is different because of a different dike pressure but the displacements within the unpressurized region is nearly identical. The dike pressure for the dike only calculation was 0.38 GPa while the dike-fault calculation used a pressure of 0.40 GPa. Figure 17 shows the fault displacement normal to the dip for both the top and bottom surface of the fault. The appearance that the fault is slightly open is more likely due to the combined coarseness of the grid and the contour algorithm than actual displacement normal the dip. The magma would bypass the fault and continue to propagate the dike upward.

### **2.6.4 Results for Depth 2 km, Dip 50°**

The grid spacing and initial conditions for these calculations was identical to the previous calculations. Figure 18 shows the grid with contours of the  $x$  displacement at the end of the dike expansion. The horizontal displacement has been magnified by a factor of 20 to better show the dike opening. The dike above the fault intersection point fractured to a depth of 1,800 m and opened to a total width of 0.1 meters at a depth of 1,900 m. The fault also opened up to a horizontal distance greater than 100 m. The displacement contours show the dike displacement below the intersection is near symmetric. Figure 19 shows the dike displacement as a function of depth. Above the intersection fault slippage caused the right side of the dike to move a smaller distance in the positive  $x$  direction than the left side moved in the negative  $x$  direction. The dike is clearly open 200 m above the intersection with the total width at the intersection being 0.35 m. Figure 20 compares the half-width displacement of the dike only calculation with the dike-fault calculation. The displacement within the pressurized region is different because a different dike pressure was used for the dike-fault calculation than the dike only calculation as was described for the 2 km- 30 degree calculation. Again the slippage of the fault caused the dike displacement above the intersection to be less than the dike only calculation. Figure 21 shows the displacement of the fault surfaces normal to the dip angle. The maximum displacement along the fault is approximately 0.12 m at the intersection. At 100 m horizontal distance the fault opening is 0.08 m. The magma would flow into both the dike and the fault. Because the opening of the vertical dike is wider

(0.35 m) and extends further (200 m) than the width (0.12 m) and extent (~ 100 m) of the opening along the fault, it is more likely the magma would continue to ascend vertically.

### **2.6.5 Results for Depth 2 km, Dip 70°**

This problem took a long time to come to equilibrium with the gravitational body forces because of slippage along the fault. The dip angle of 70° was much greater than the coefficient of friction on the fault surface. The results from Depth 1 km, Dip 50° are very similar with this calculation as was expected, consequently the slippage did not seem to effect the calculational results. Figure 22 shows the grid at maximum dike displacement with horizontal displacement contours and shows the dike above the fault closed and unfractured. The horizontal displacement has been magnified by a factor of 20 to better show the dike opening. The contours show that the dike below the intersection is non-symmetric where matching contours are offset by more than 100 m. The fault is open and extends past 100 m. Figure 23 shows the dike displacement as a function of depth. The unbroken bonds on the dike above the intersection caused the right hand side to slip along the fault and move with the left hand side of the dike. Figure 24 shows the comparison of the dike only displacement with the dike-fault displacement. There is good agreement between the two except for the region above the fault intersection. Figure 25 shows the fault displacement as a function of horizontal distance from the dike. The upper curve is the top surface of the fault, the lower curve is the bottom surface of the fault. The opening of the fault is on the order of 0.40 m and would support magma flow beyond a 100 m, horizontal distance.

### **2.6.6 Results for Depth 5 km, Dip 70°**

In the modeling at a depth of 5 km, the slippage was so much that the bonds above the dike broke in shear as one side of the dike settled more than the other side. The calculation was continued to determine how critical the tensile strength above the fault was for this case. At the time that the magma pressure began to expand the dike, the effective tensile strength across the dike above the fault intersection was zero. Figure 26 shows the grid at maximum dike wall displacement with horizontal displacement contours. The horizontal displacement has been magnified by a factor of 20 to better show the dike opening. The fault and dike make one continuous open path for the magma. The dike path just above the fault is closed but fractured. Figure 27 shows the dike displacement with depth. Similar to all the calculations where the dike terminated at the intersection, the dike path shifted to the left and the fault slippage at the intersection is apparent in the displacement of the dike walls at that point. The top surface of the fault moved to the left and the lower surface of the fault moved to the right. Figure 28 shows the comparison of the dike only displacement with the dike-fault displacement. There is good agreement between the two except for the region above the fault intersection. Figure 29 shows the fault displacement normal to the dip as a function of horizontal distance from the dike. The fault opening is greater than 0.2 m at the intersection and 0.1 m wide as far in as 100 m from the dike.

At the intersection, the dike width is 0.05 m. In spite of the dike path failure above the intersection before the dike pressure was applied, the dike remained closed due to the high overburden pressure and slippage of the top of the fault to the left. The magma would travel up the fault and the dike would cease to propagate.

### **2.6.7 Results for Depth 5 km, dip 50° Calculation**

The slippage along the fault was negligible and unlike the 70° dip calculation, the bonds on the dike above the fault intersection remained intact. The dike opened up about 20 m above the intersection with a width of 0.2 m at the intersection. Figure 30 shows the grid at maximum dike wall displacement with horizontal displacement contours. The horizontal displacement has been magnified by a factor of 20 to better show the dike opening. The fault and dike make one continuous open path for the magma. The dike path just above the fault is open to 20 m above the intersection and unfractured above that. Figure 31 shows the dike displacement with depth. Similar to all the calculations where the dike terminated at the intersection, the dike path shifted to the left but remained tightly closed. The dike opening is approximately 0.2 m at the intersection. Figure 32 shows the comparison of the dike only displacement with the dike-fault displacement. There is good agreement between the two except for the region above the fault intersection. Figure 33 shows the fault displacement normal to the dip as a function of horizontal distance from the dike. The fault opening is approximately 0.2 m at the intersection but tapers down to 0.1 m wide at 60 m from the dike.

The magma would travel up the fault a short distance then freeze in the region where the fault opening narrows. The dike pressure would then begin to work on the dike again and continue to propagate upward.

### 3 CONCLUSIONS

The deflection of the magma along a intersected fault depends on the size of the fault opening and the lack of continuation of the dike fracture past the dike-fault intersection. In terms of whether the magma is deflected by the fault or not, the results from the simulations were very similar to the results from the analytical study of Connor et al. (1994). At 1 km the curve of Connor et al. (1994) (figure 1) gives the transition from dike flow to fault flow at a dip of  $40^\circ$ . The simulations indicate the transition above fault dip  $30^\circ$  and below fault dip  $50^\circ$ . At 2 km the transition is at fault dip  $58^\circ$ . The simulations at 2 km depth indicate the transition is very close to but above the fault dip  $50^\circ$ , since this calculation shows simultaneous opening along both the fault and the dike above the fault, but below a fault dip of  $70^\circ$ . At 5 km, Connor et al. (1994) indicate the transition is at  $70^\circ$ . The simulation indicates the transition is below fault dip  $70^\circ$ . The opening of the fault at  $50^\circ$  dip could result in an offset in the dike where the magma went up the fault a short way, then branched off to a new vertical fracture and continued upward.

## 4 REFERENCES

- Connor, C.B., S. McDuffie, and B.E. Hill. 1994. Field volcanism research. *NRC High-Level Radioactive Waste Research at CNWRA July-December 1993, Chapter 10*. B. Sagar, ed. CNWRA. San Antonio, Texas: Center for Nuclear Waste Regulatory Analyses.
- Pollard, D.D. 1987. Elementary fracture mechanics applied to the structural interpretation of dykes. *Geological Association of Canada Special Papers* 34: 5-24.
- Whirley, R., and J.O. Hallquist. 1991. *DYNA3D A Nonlinear, Explicit, Three-dimensional Finite Element Code for Solid and Structural Mechanics: User Manual UCRL-MA-107254*.

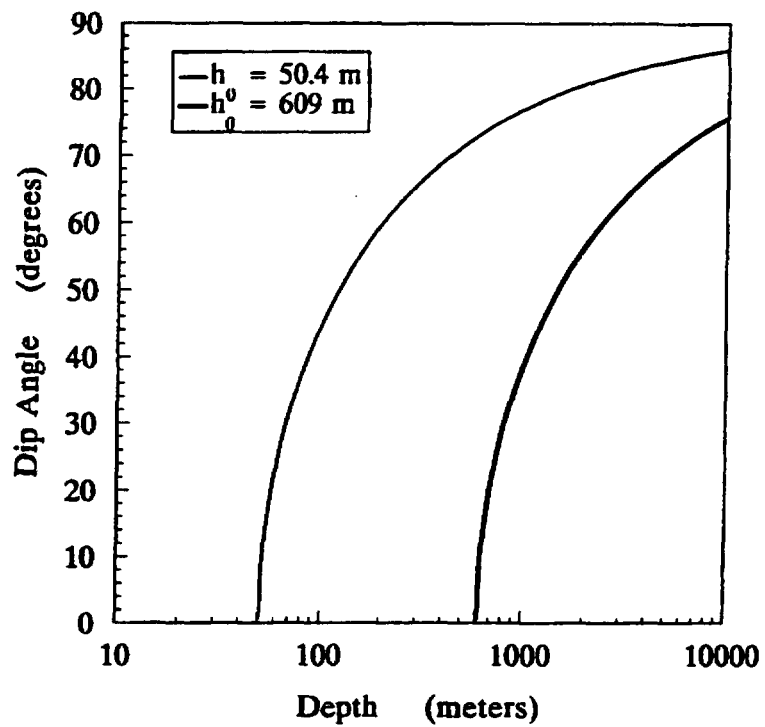


**Figure 1.** The minimum dip angle of a fault that will redirect an upwardly propagating dike is a function of depth and rock properties. The curve for  $h_0 = 609$  m is for a tensile strength of 10 MPa. Calculation of  $h$  for the material properties of this study gave  $h_0 = 588$  m (Connor et al. 1994).

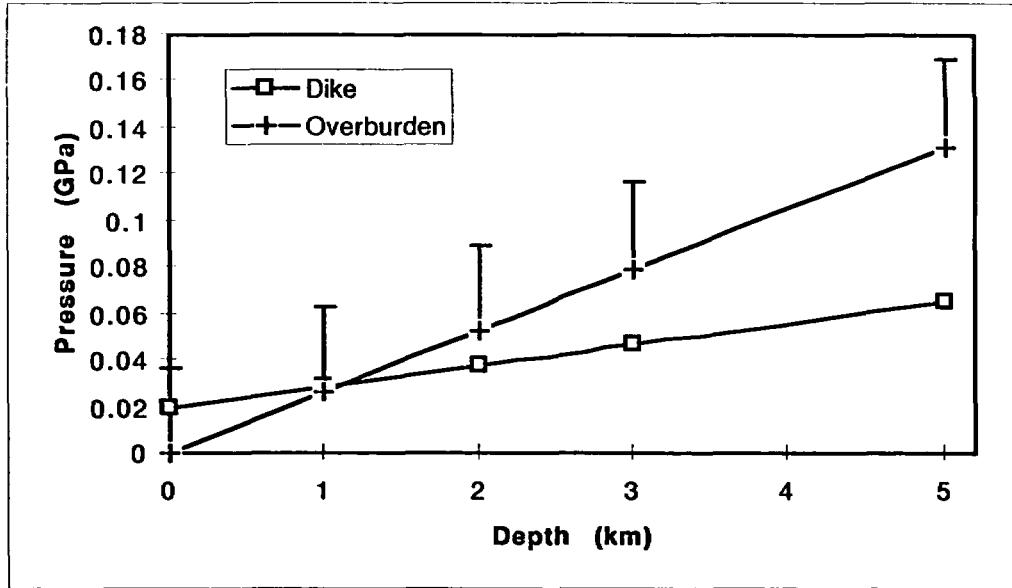


**Figure 2. Comparison of pressure needed to open dike to the overburden pressure as a function of depth. The total dike width is approximately 1 m in all cases.**

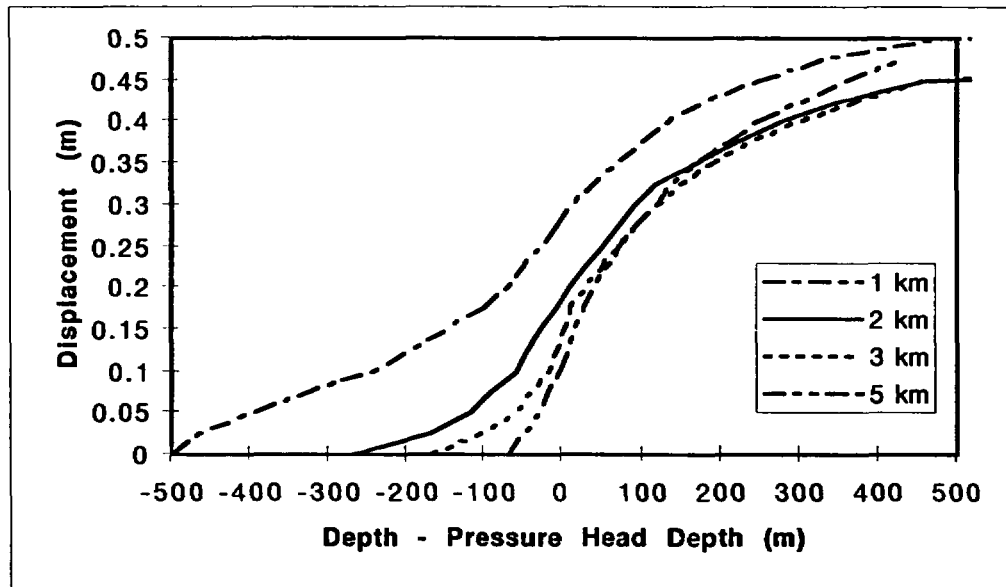


**Figure 3. Dike crack shape vs. depth for four depths in absence of fault**

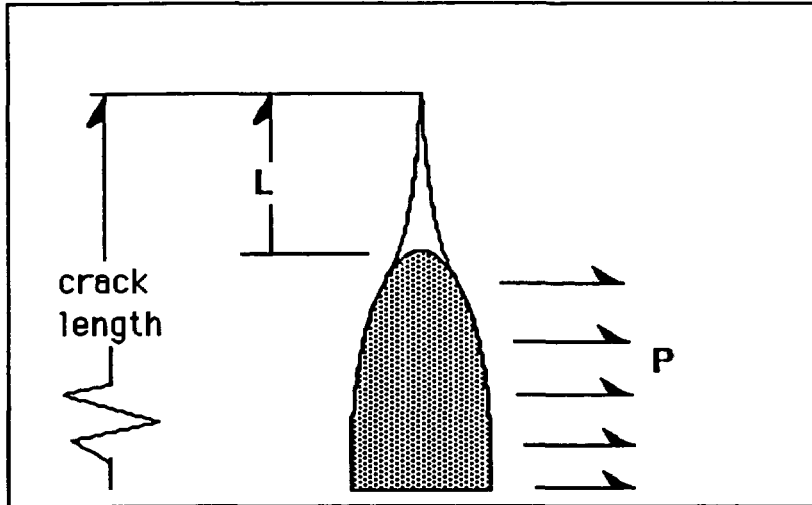


**Figure 4. The cohesive zone model. Magma pressure  $P$  is exerted on the dike wall except over a small length  $L$  at the dike tip.**

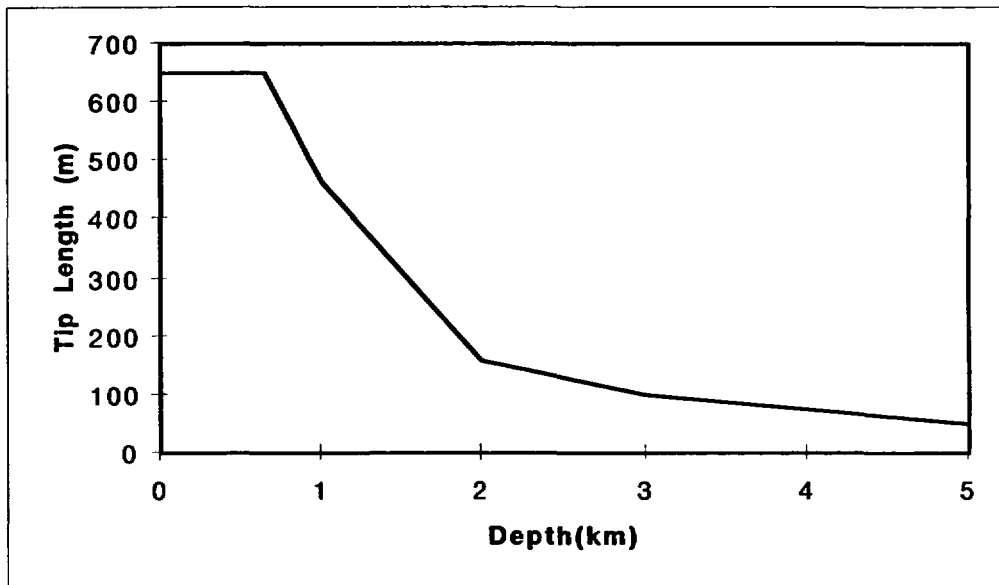


**Figure 5. Length of dike tip  $L$  as a function of depth. When the dike pressure head is at 650 m, the dike tip reaches the surface.**

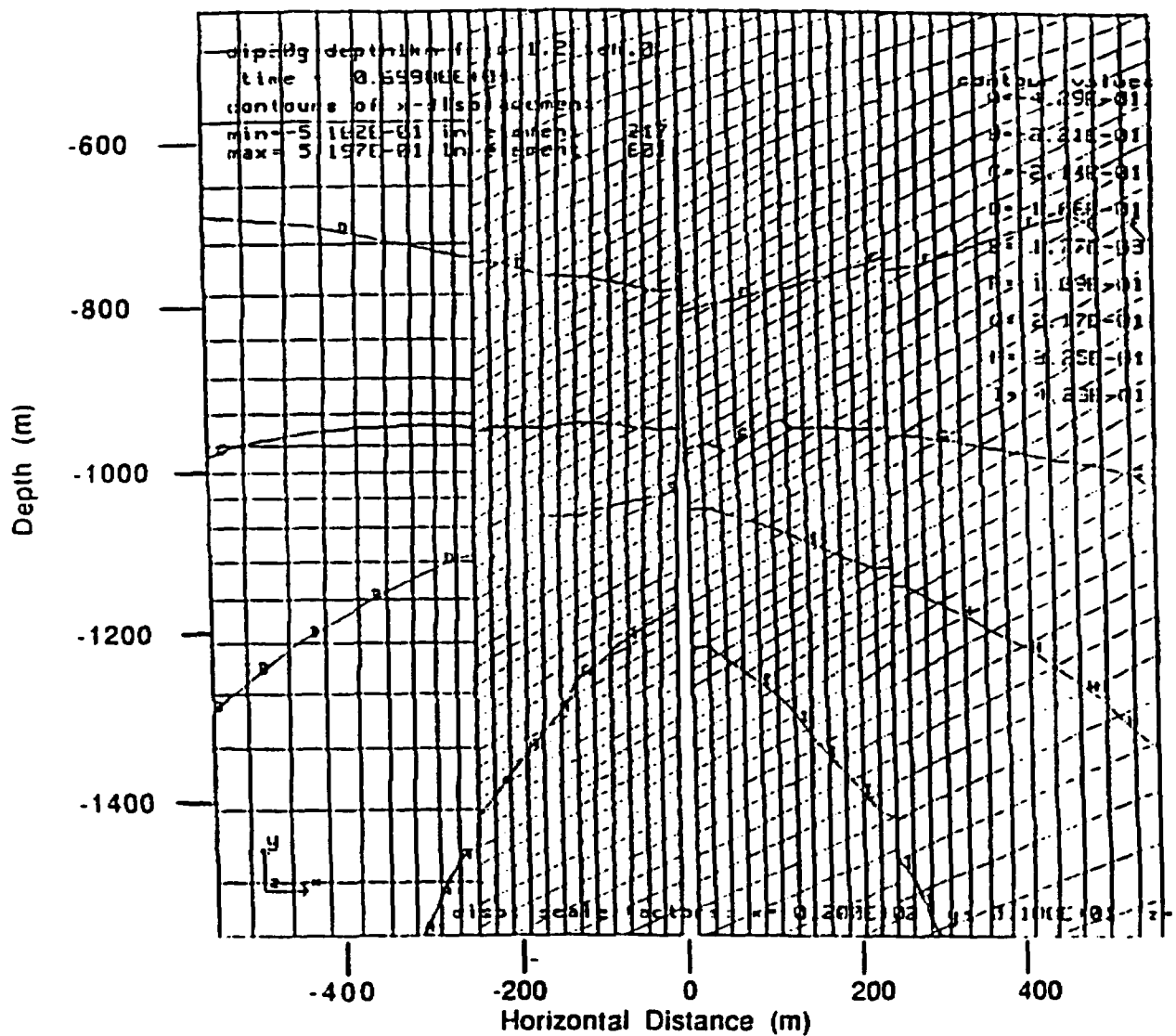


**Figure 6. Depth = 1 km, dip = 30 degrees. Grid with horizontal displacement contours showing the dike, fault configuration after maximum dike wall displacement. The grid is zoned to the surface. The fault is terminated 1 km from the dike on the right, and 240 m on the left. Horizontal displacement was magnified by a factor of 20 to better show dike displacement.**

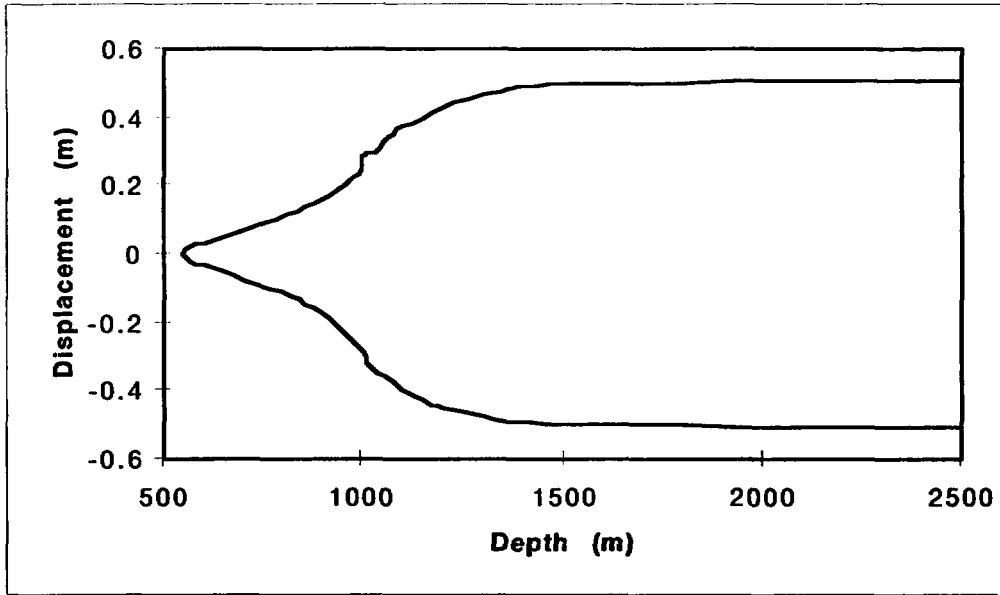


Figure 7. Dike displacement as a function of depth for dike-fault at depth = 1 km and dip = 30 degrees. The displacement is symmetrical about the dike plane.

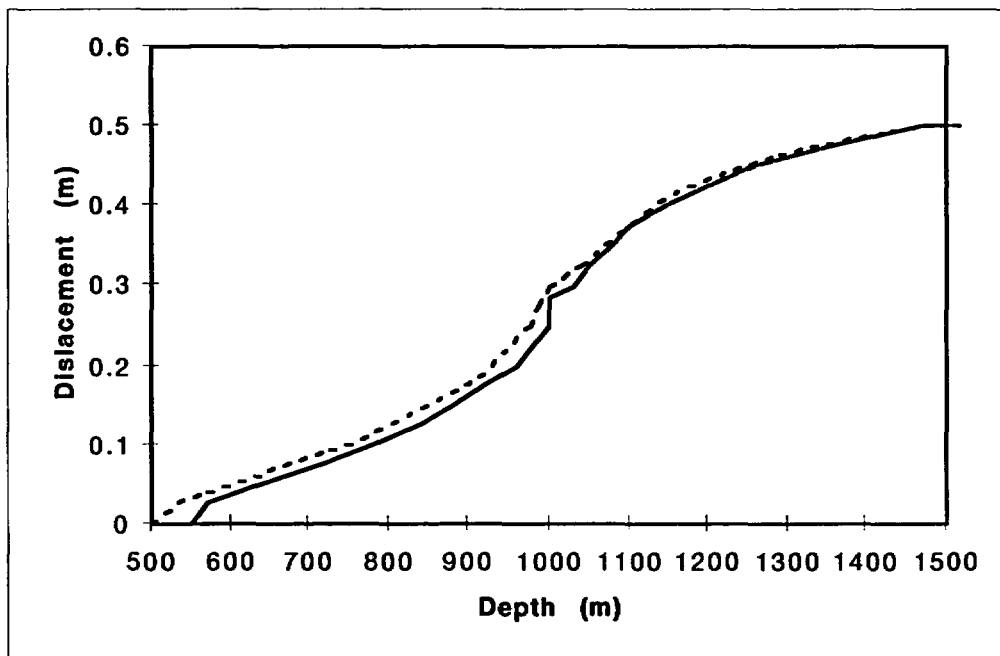
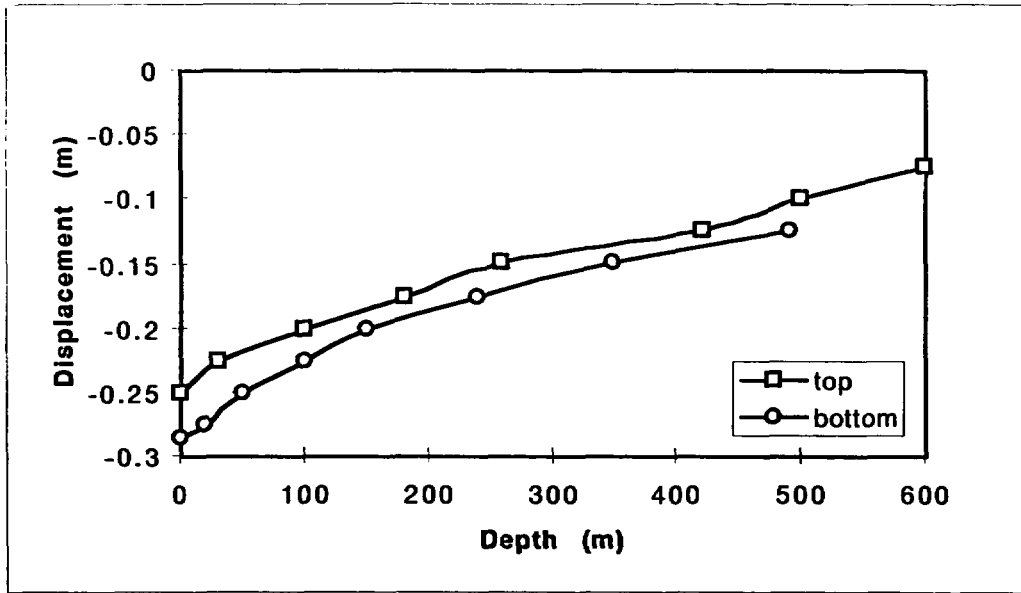
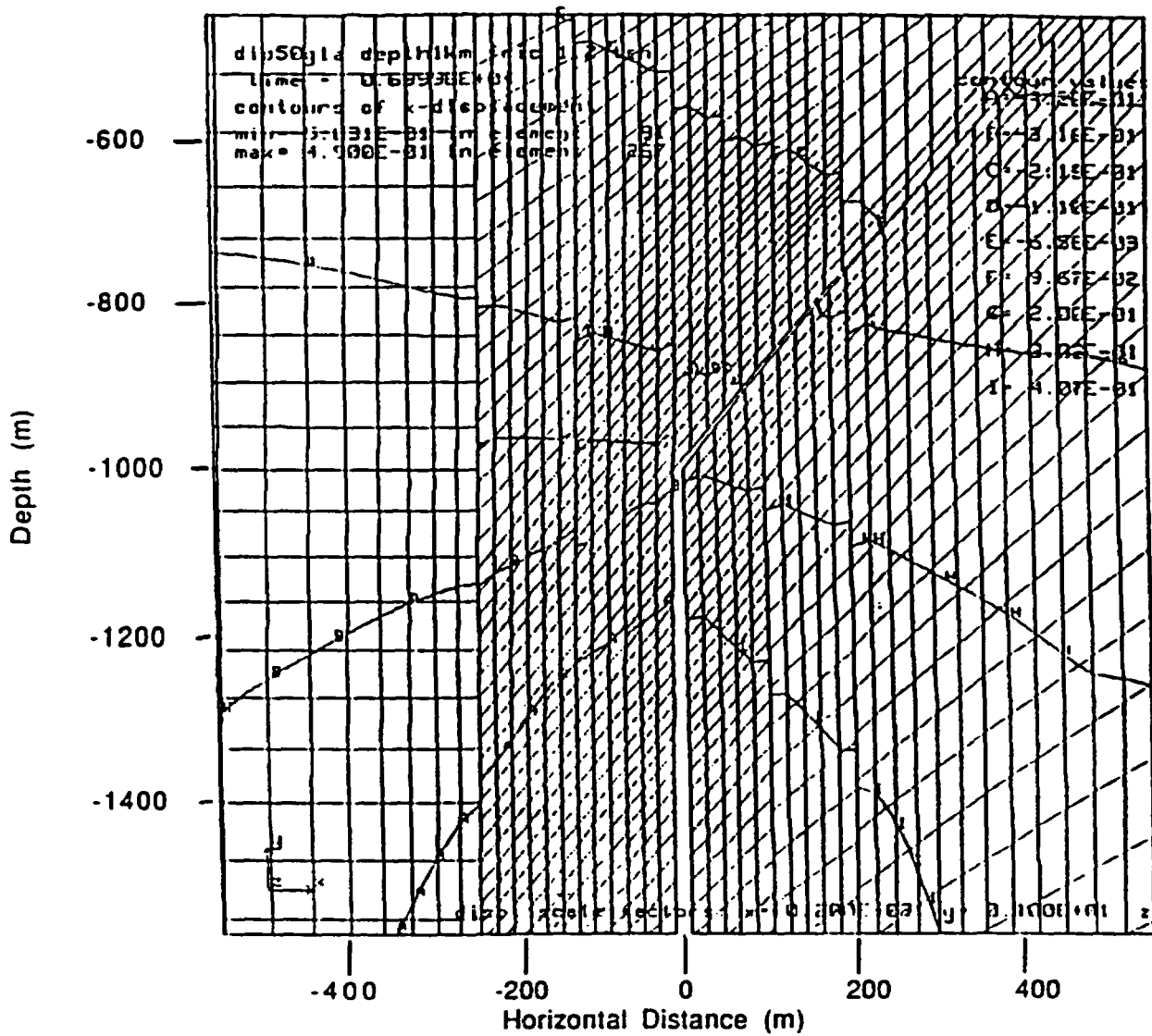


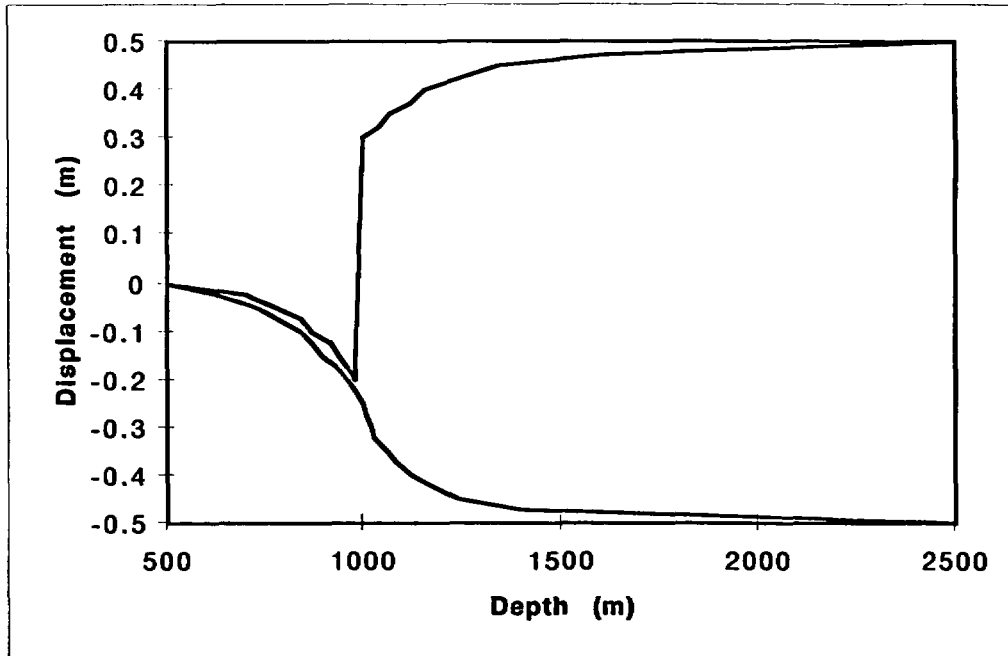
Figure 8. Comparison of dike only (dotted line) to dike-fault for dip = 30 degrees (solid line), both at depth = 1 km



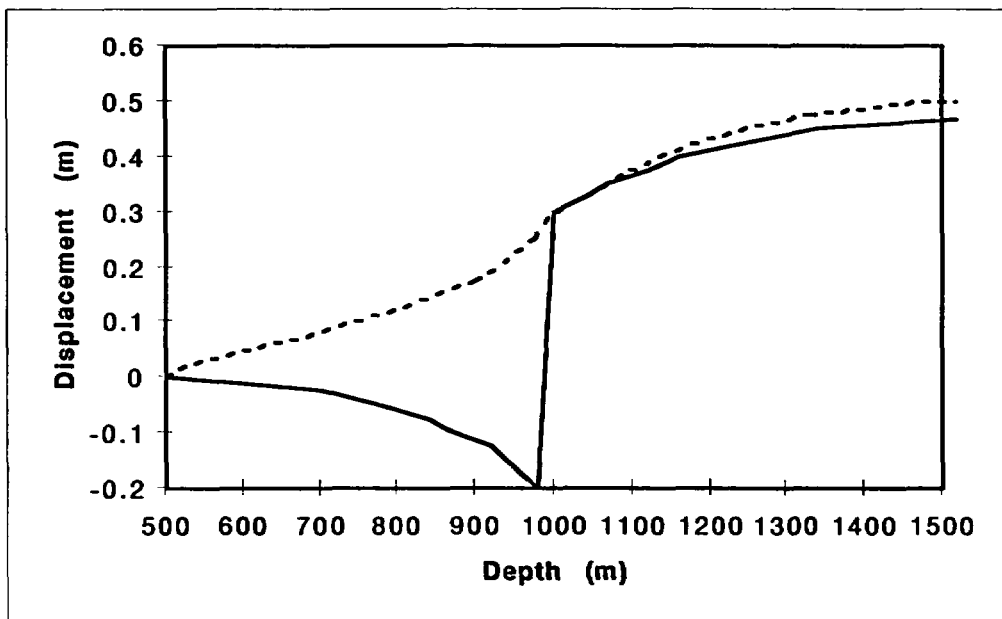
**Figure 9. Fault displacement normal to the dip at depth = 1 km and dip = 30 degrees. This fault is essentially closed.**



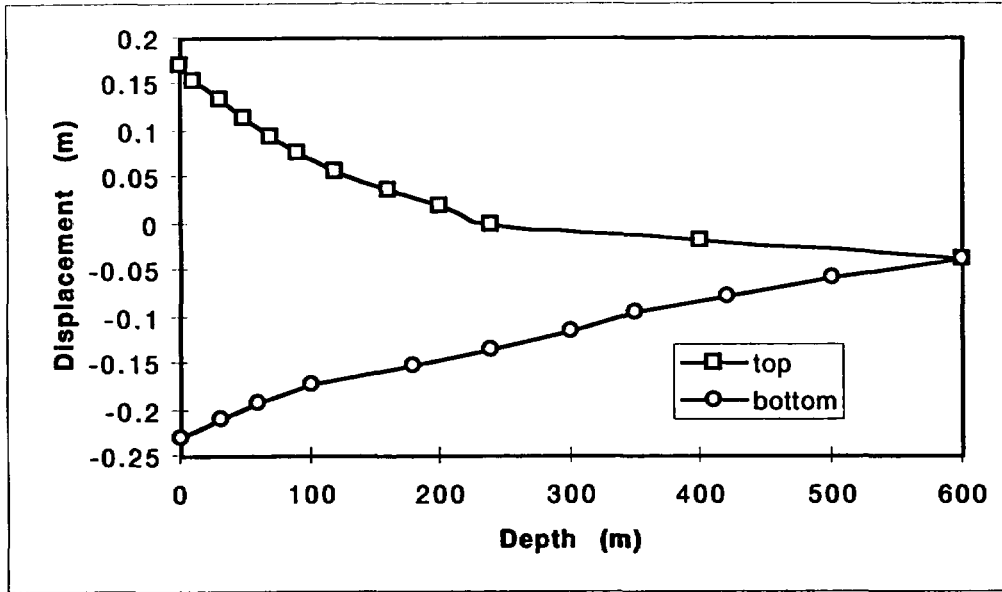
**Figure 10. Depth = 1 km, dip = 50 degrees. Grid with horizontal displacement contours showing the dike, fault configuration after maximum dike wall displacement. The grid is zoned to the surface. The fault is terminated 600 m from the dike on the right, and 240 m on the left. Horizontal displacement was magnified by a factor of 20.**



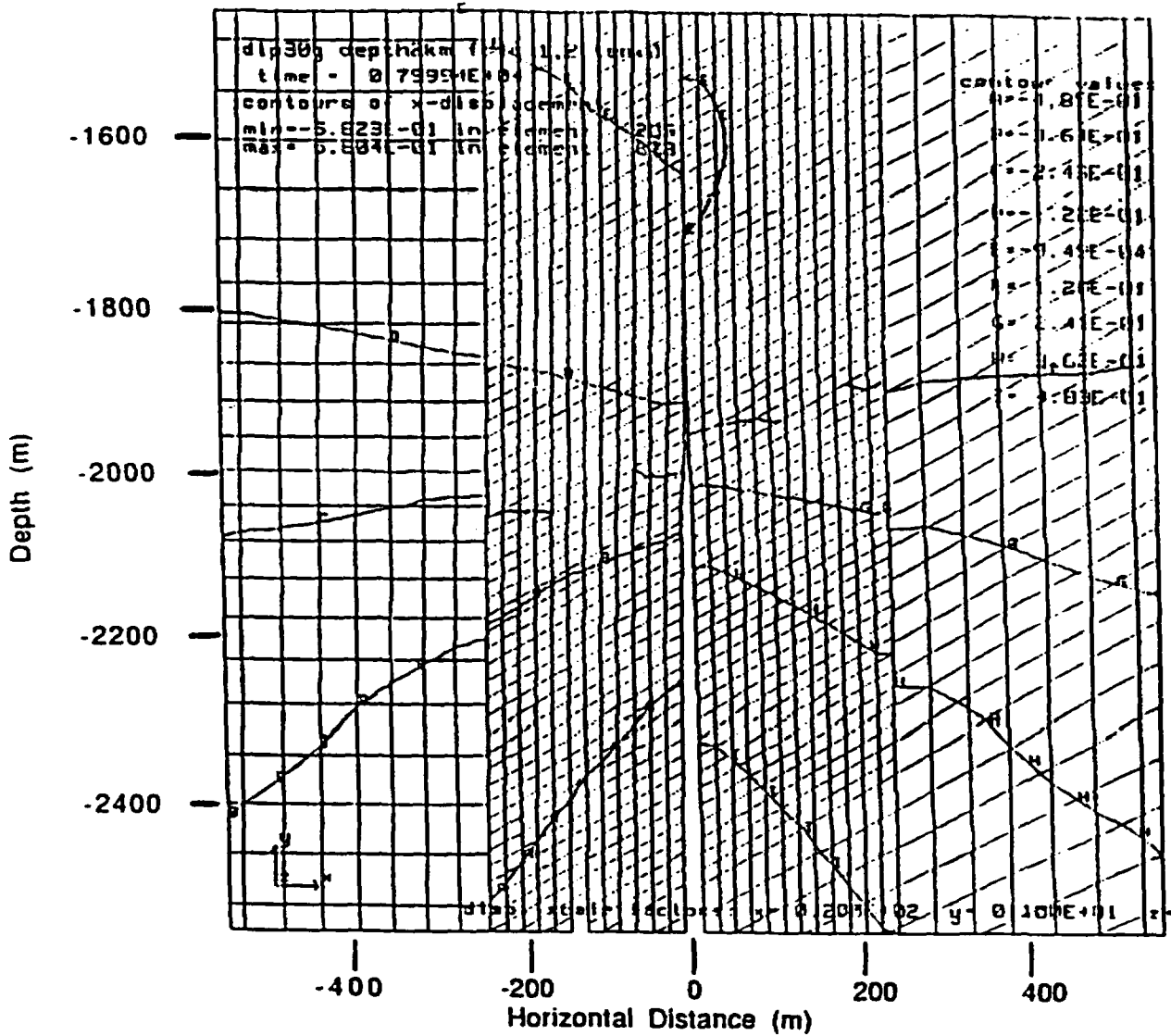
**Figure 11.** Dike displacement as a function of depth for dike-fault at depth = 1 km and dip = 50 degrees. The dike fracture above the fault is essentially closed.



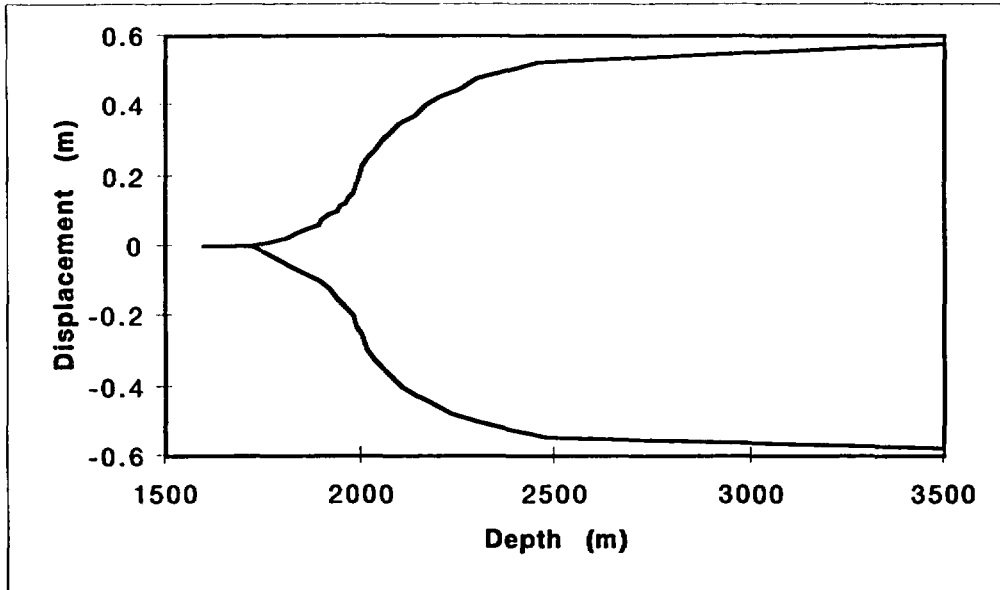
**Figure 12.** Comparison of dike only (dotted line) to dike-fault with dip = 50 degrees (solid line), both at depth = 1 km



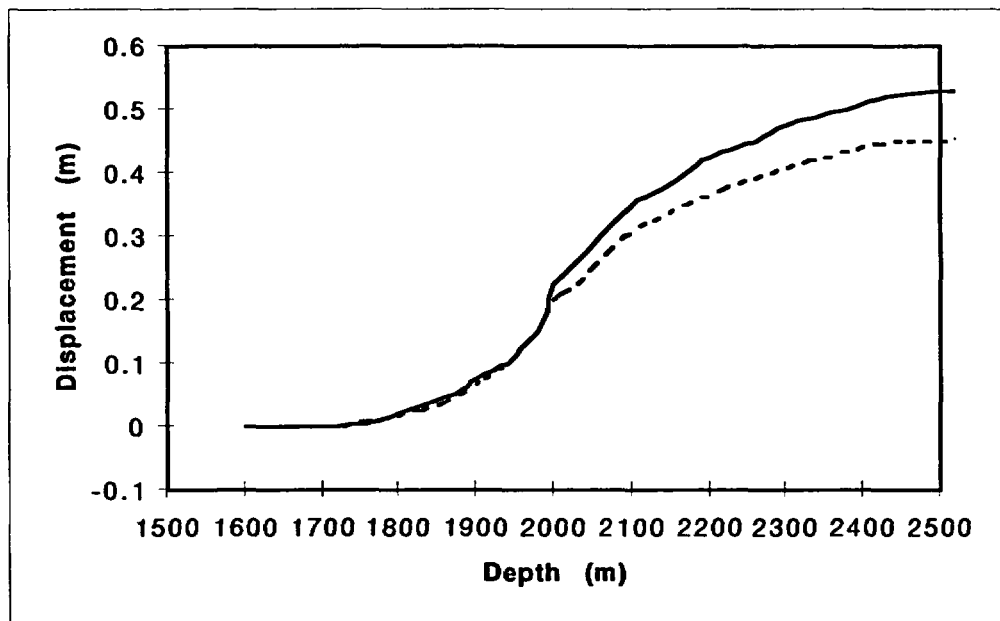
**Figure 13. Fault displacement normal to the dip at depth = 1 km and dip = 50 degrees. The fault is open 0.4 m at its intersection with the dike.**



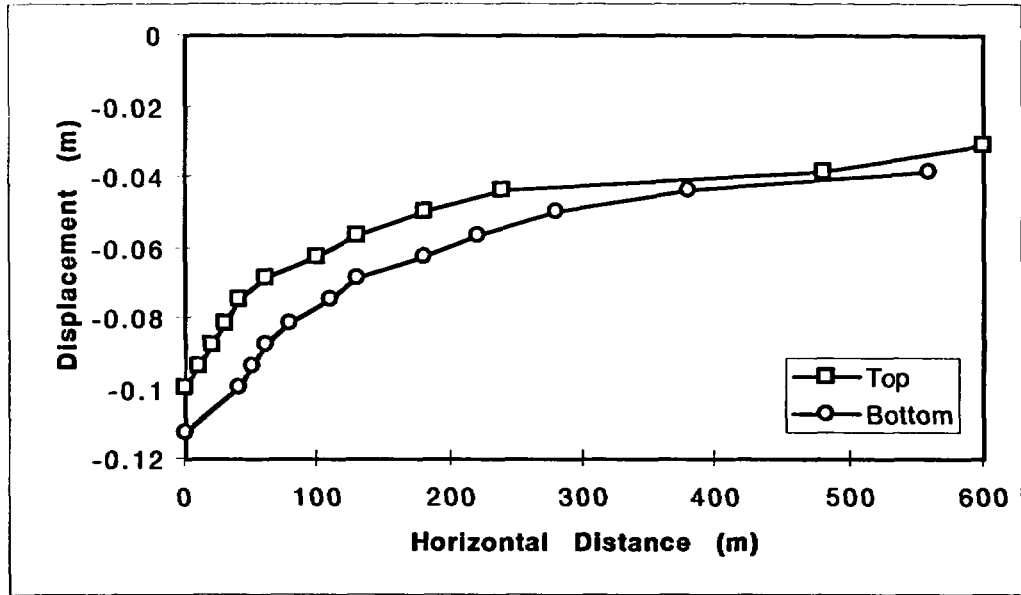
**Figure 14. Depth = 2 km, dip = 30 degrees. Grid with horizontal displacement contours showing the dike, fault configuration after maximum dike wall displacement. The grid is zoned to the surface. The fault is terminated 1 km from the dike on the right, and 240 m on the left. Horizontal displacement was magnified by a factor of 20.**



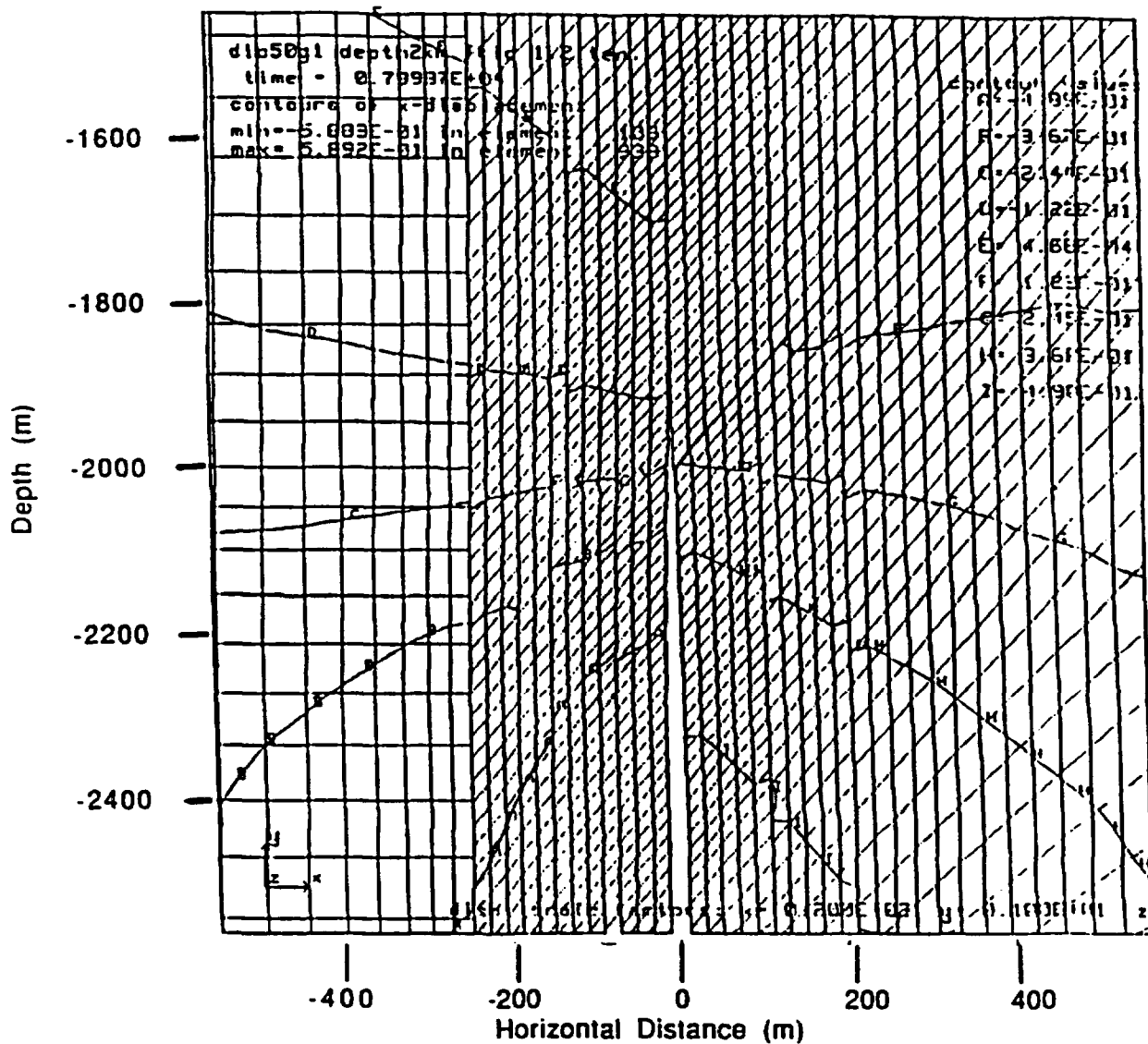
**Figure 15. Dike wall displacement for dike-fault calculation at depth = 2 km and dip = 30 degrees**



**Figure 16. Comparison of dike wall half-width displacement for dike-only simulation (dotted line) to dike-fault simulation (solid line) at depth = 2 km and fault dip = 30 degrees**



**Figure 17. Fault displacement normal to dip for dike-fault simulation at depth = 2 km and dip = 30 degrees**



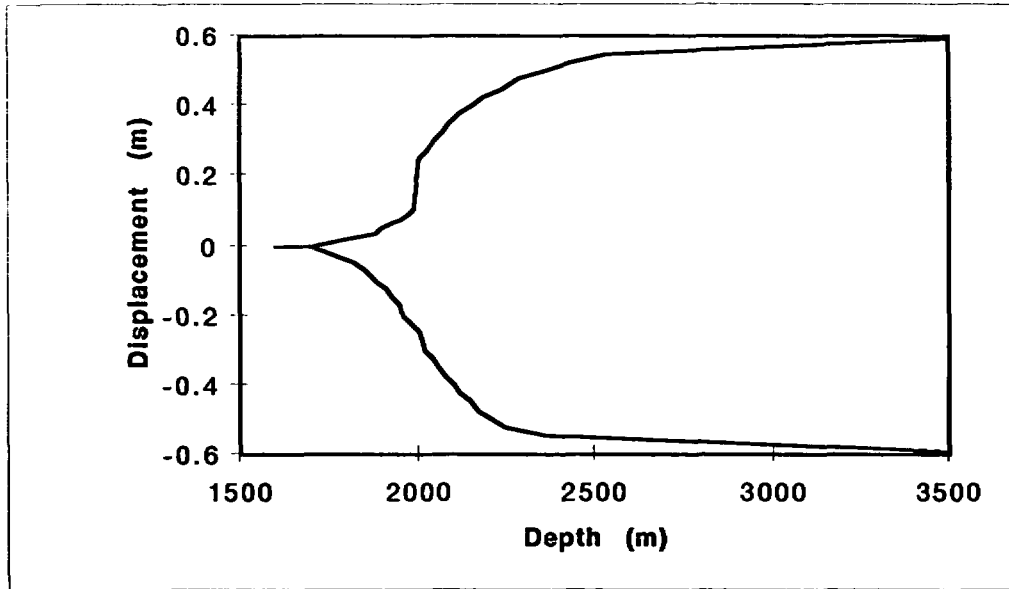


**Figure 19.** Dike wall displacement as function of depth for dike-fault simulation at depth = 2 km and dip = 50 degrees

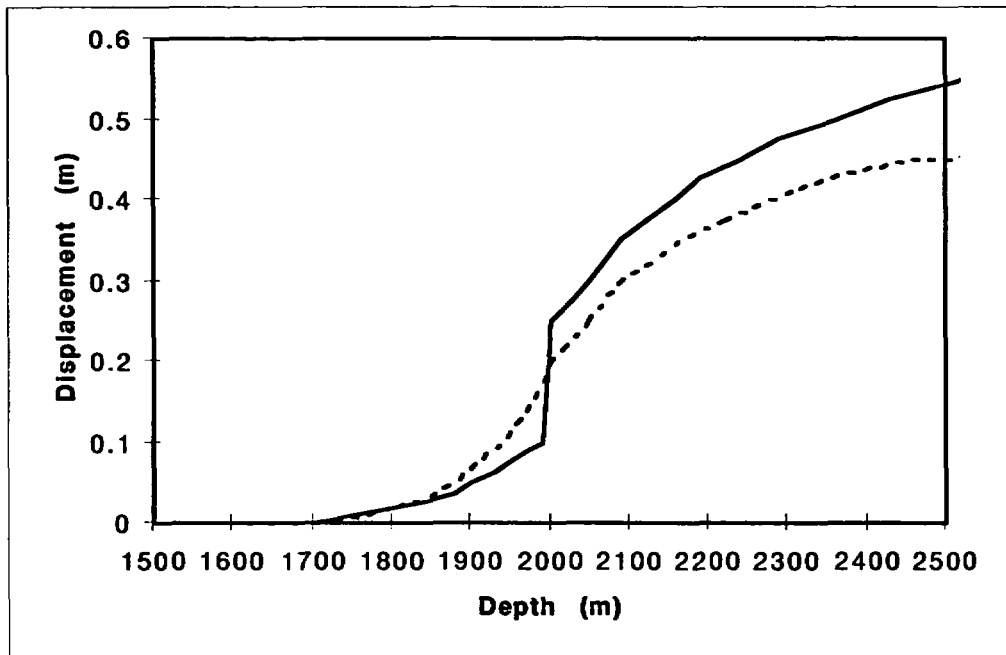


**Figure 20.** Comparison of dike wall half-width displacement for dike-only simulation (dotted line) to dike-fault simulation (solid line) at depth = 2 km and fault dip = 50 degrees

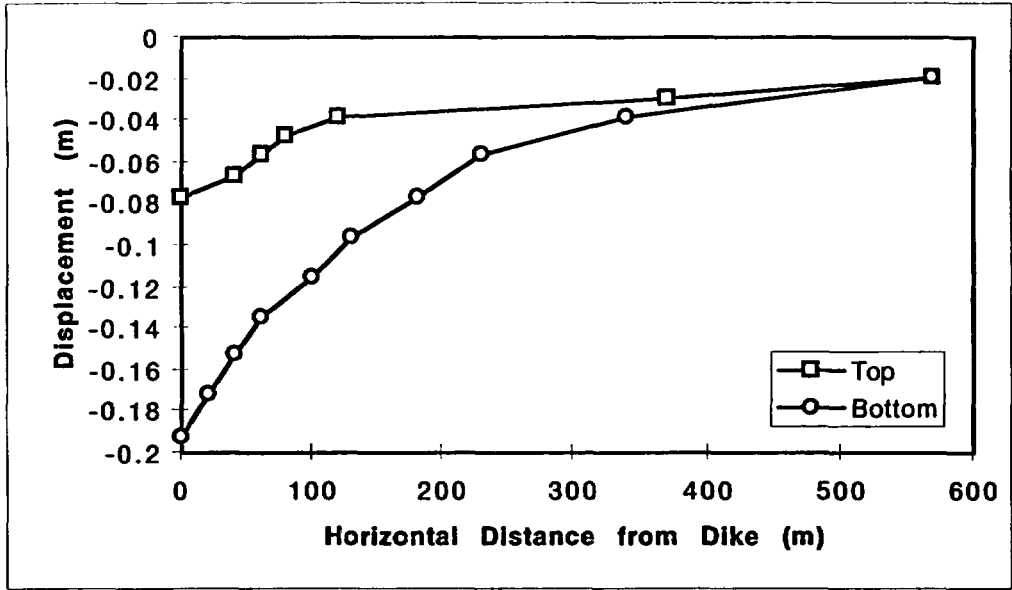


**Figure 21. Fault displacement normal to dip for dike-fault simulation at depth = 2 km and dip = 50 degrees**

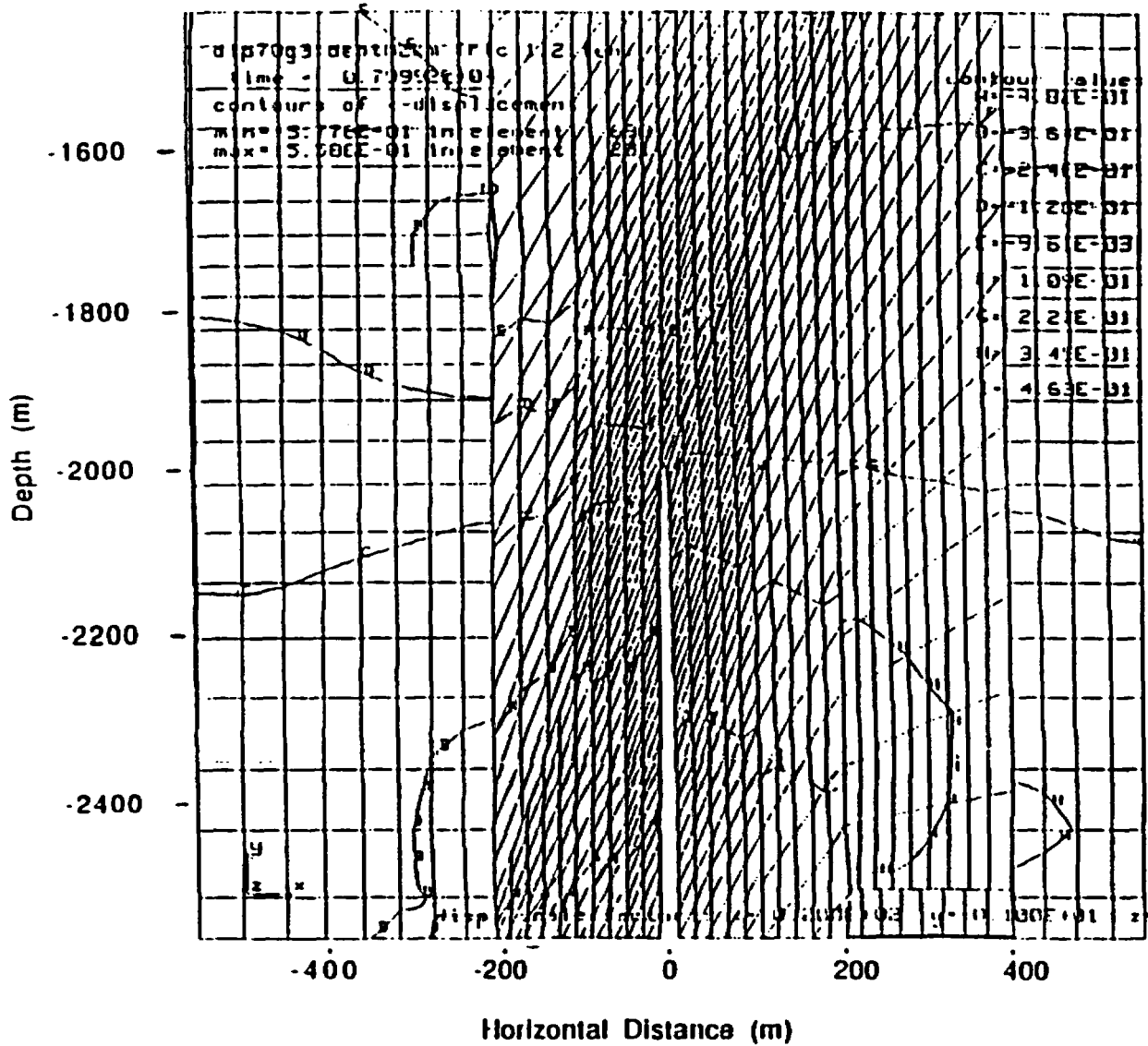


**Figure 22. Depth = 2 km, dip = 70 degrees. Grid with horizontal displacement contours showing the dike, fault configuration after maximum dike wall displacement. The grid is zoned to the surface. The fault is terminated 400 m from the dike on the right, and 200 m on the left. Horizontal displacement was magnified by a factor of 20.**

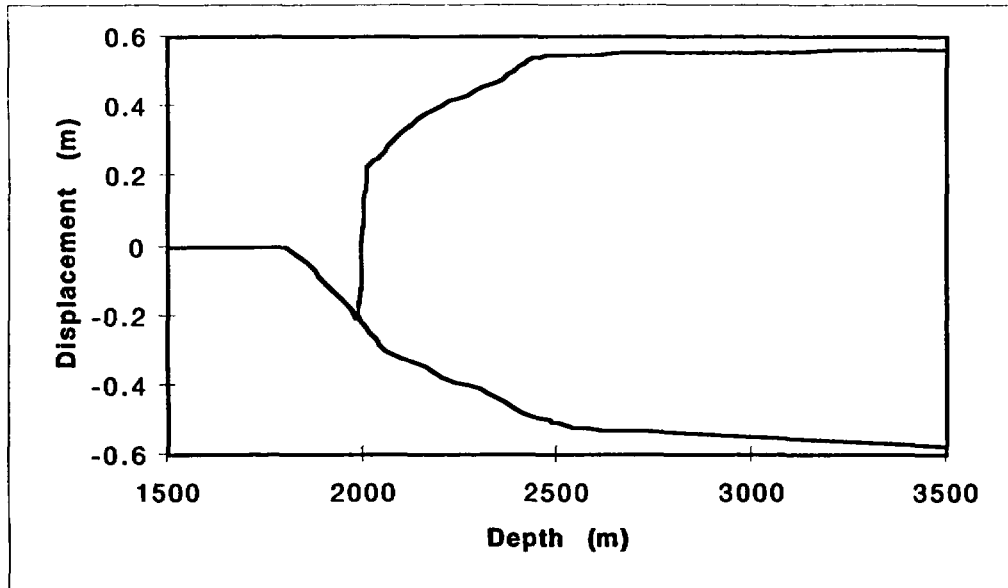


**Figure 23. Dike wall displacement as a function of depth for dike-fault simulation at depth = 2 km and dip = 70 degrees**

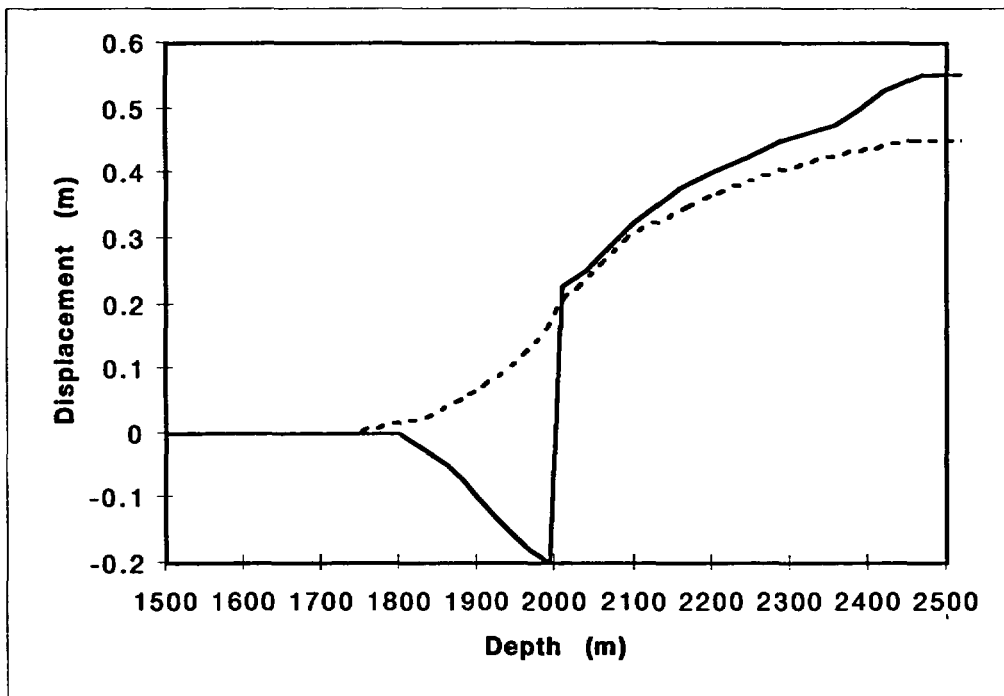


**Figure 24. Comparison of dike wall half-width displacement for dike-only simulation (dotted line) to dike-fault simulation (solid line) at depth = 2 km and fault dip = 70 degrees**

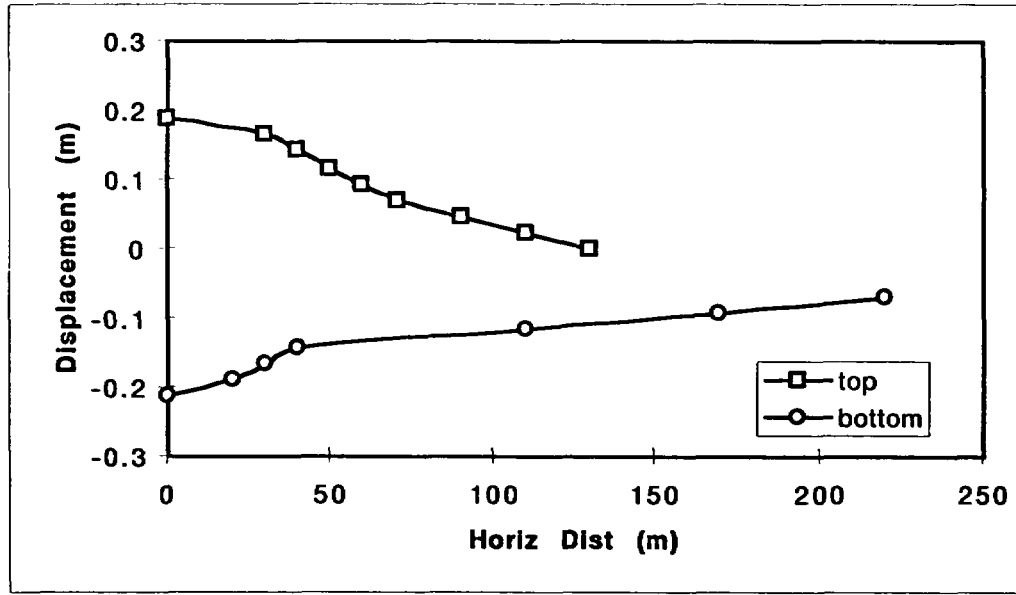


**Figure 25. Fault displacement normal to dip for dike-fault simulation at depth = 2 km and dip = 70 degrees**

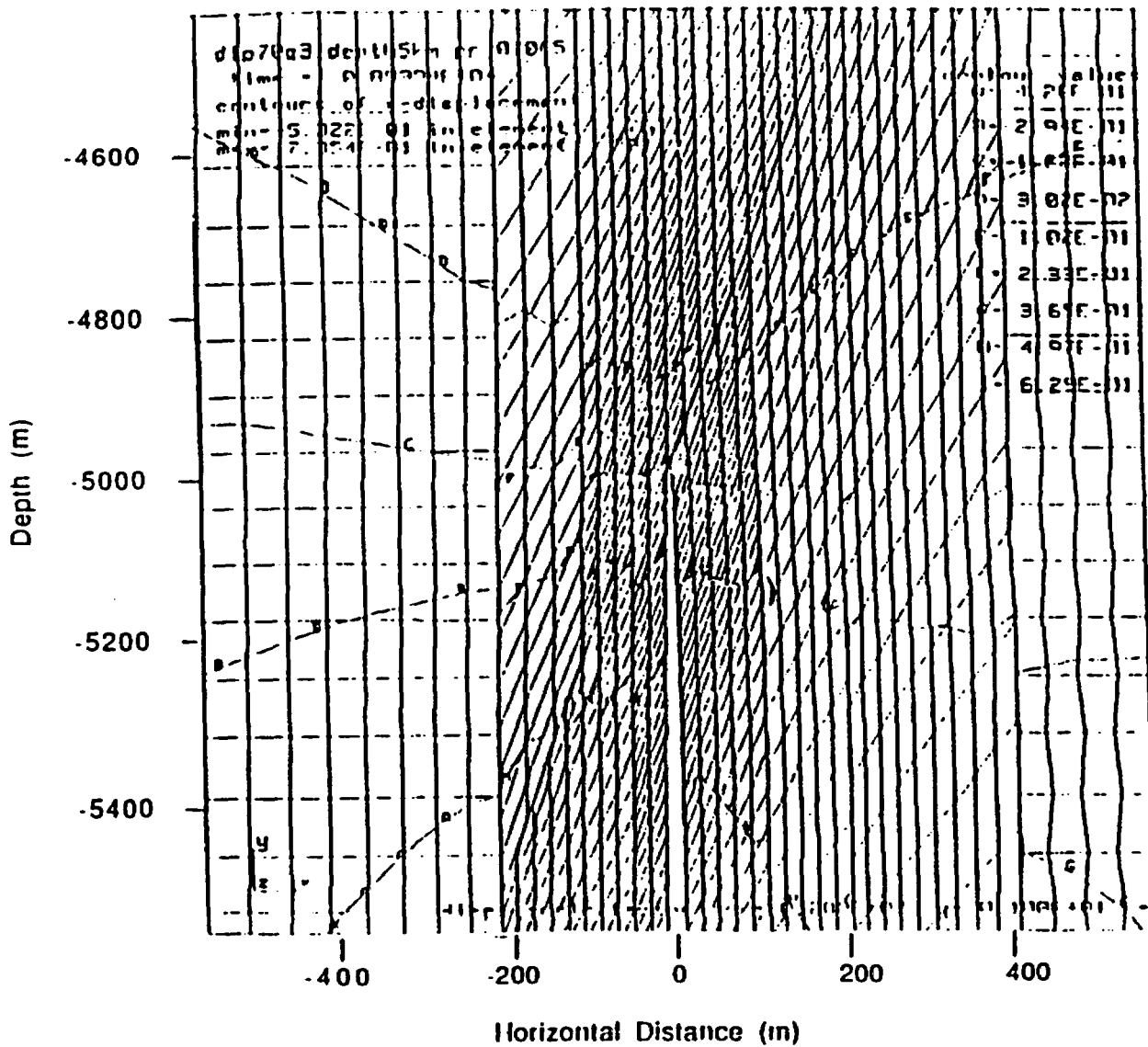
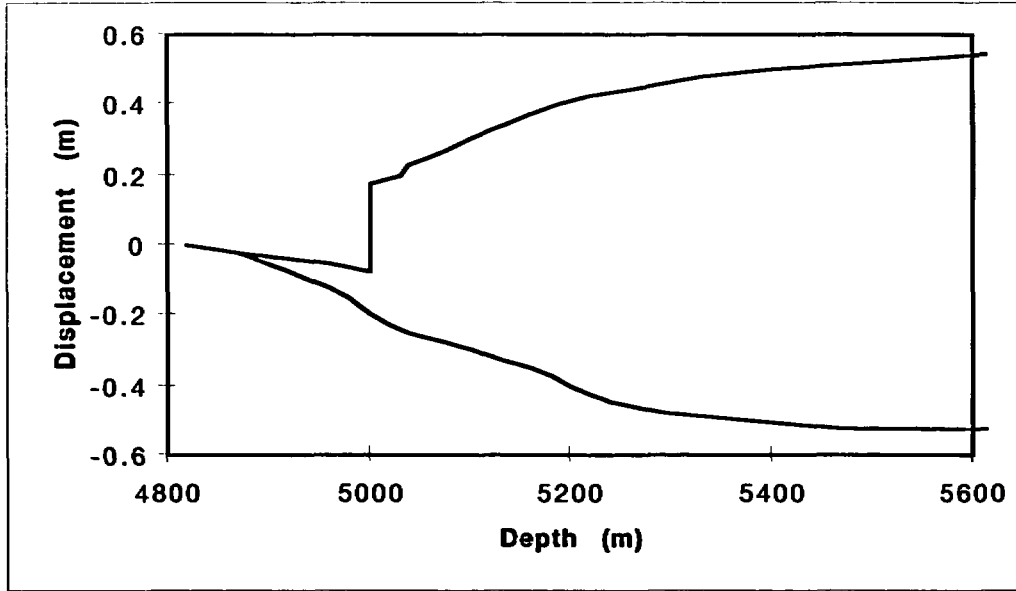
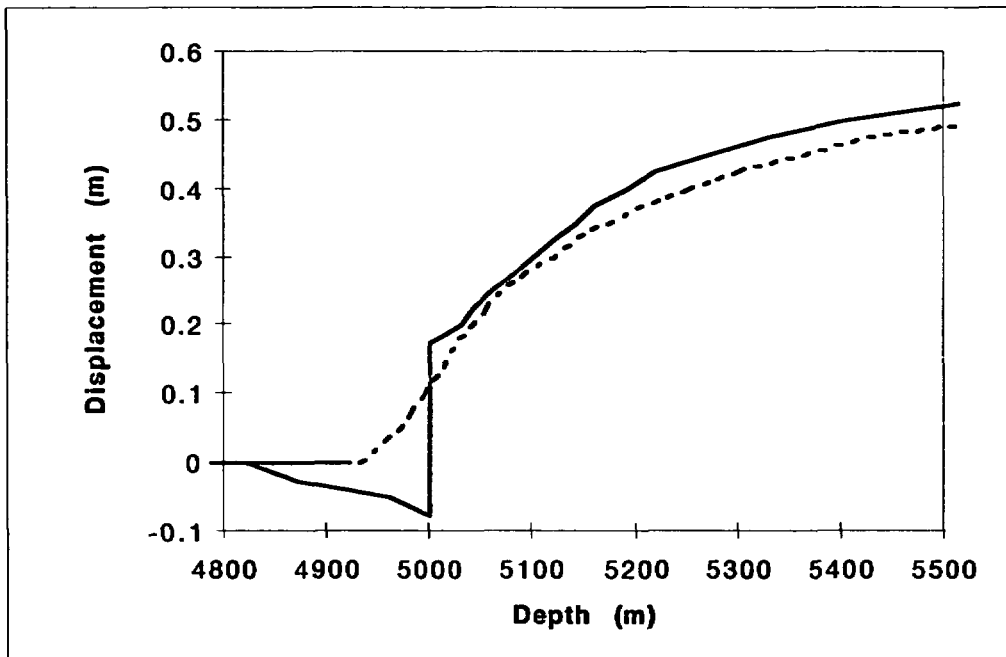


Figure 26. Depth = 5 km, dip = 70 degrees. Grid with horizontal displacement contours showing the dike, fault configuration after maximum dike wall displacement. The grid is zoned to the surface. The fault is terminated 400 m from the dike on the right, and 200 m on the left. Horizontal displacement was magnified by a factor of 20.



**Figure 27. Dike wall displacement as a function of depth for dike-fault simulation at depth = 5 km and dip = 70 degrees**



**Figure 28. Comparison of dike wall half-width displacement for dike-only simulation (dotted line) to dike-fault simulation (solid line) at depth = 5 km and dip = 70 degrees**

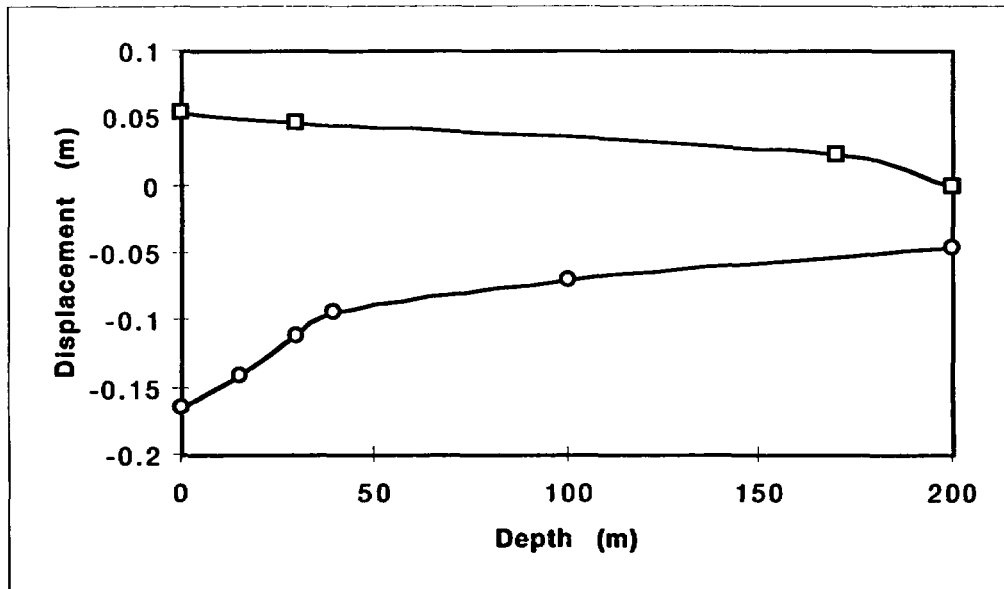


**Figure 29. Fault displacement normal to dip for dike-fault simulation at depth = 5 km and dip = 70 degrees**

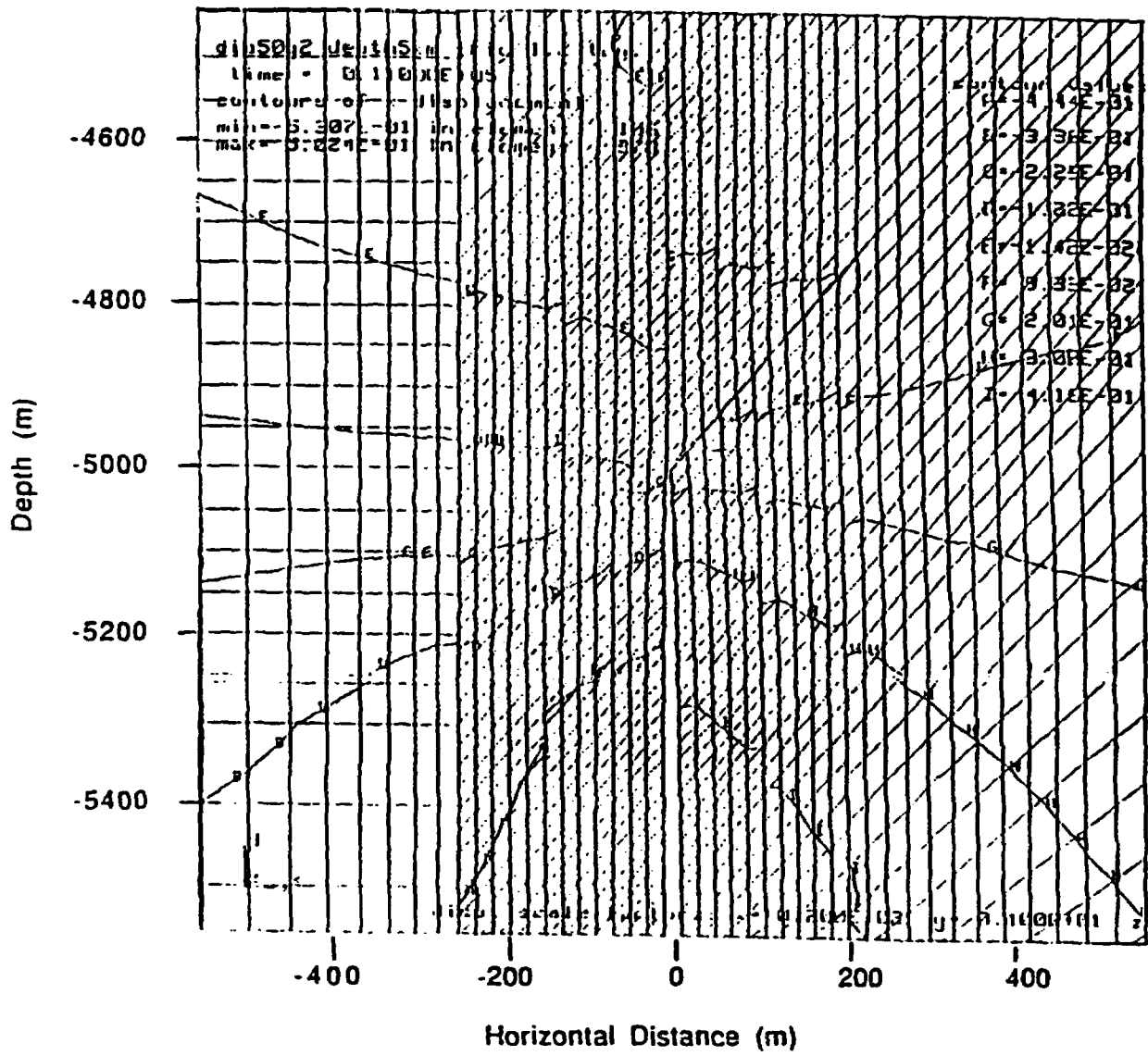


**Figure 30. Depth = 5 km, dip = 50 degrees. Grid with horizontal displacement contours showing the dike-fault configuration after maximum dike wall displacement . The fault terminated 600 m from dike on the right and 200 m on the left. Dike pressure was 0.065 GPa. Horizontal displacement was magnified by a factor of 20.**

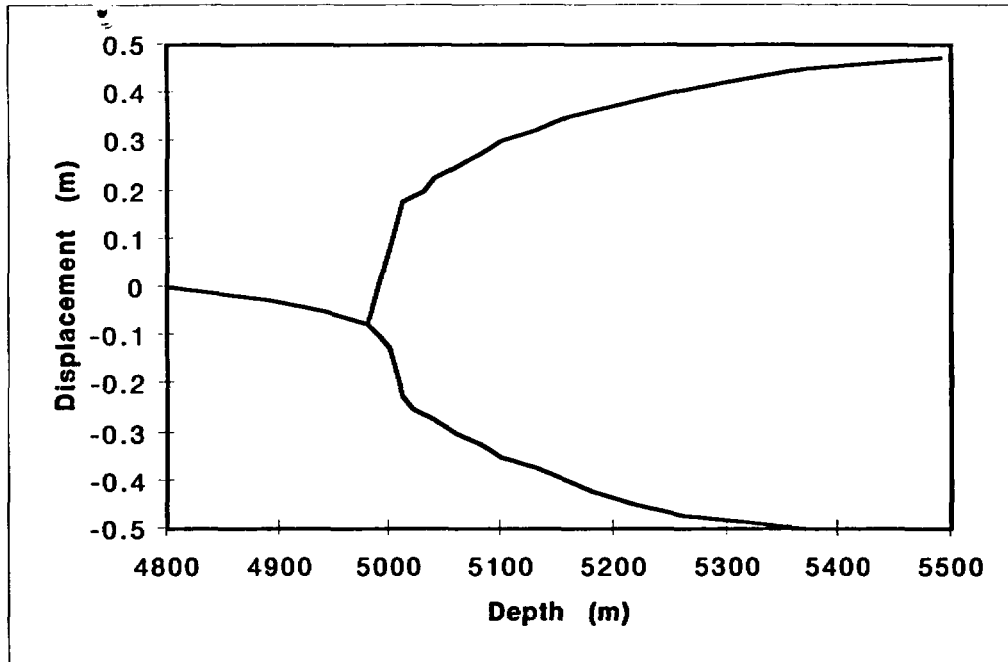


**Figure 31. Dike displacement at depth = 5 km and dip = 50 degrees**

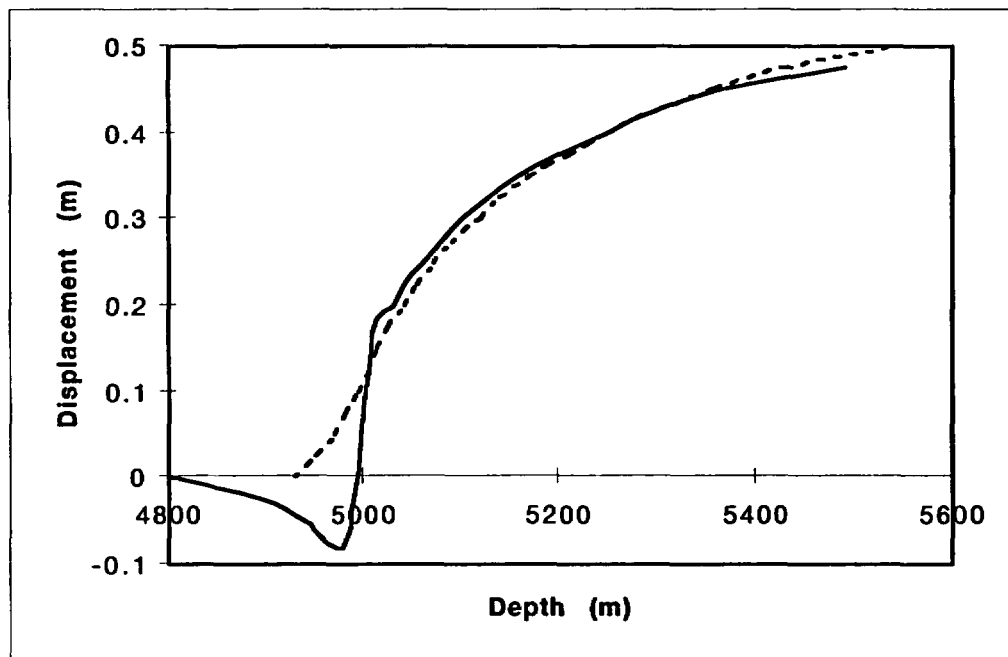


**Figure 32. Comparison of dike wall half-width displacement for dike-only simulation (dotted line) to dike-fault simulation (solid line) at depth = 5 km and dip = 50 degrees**

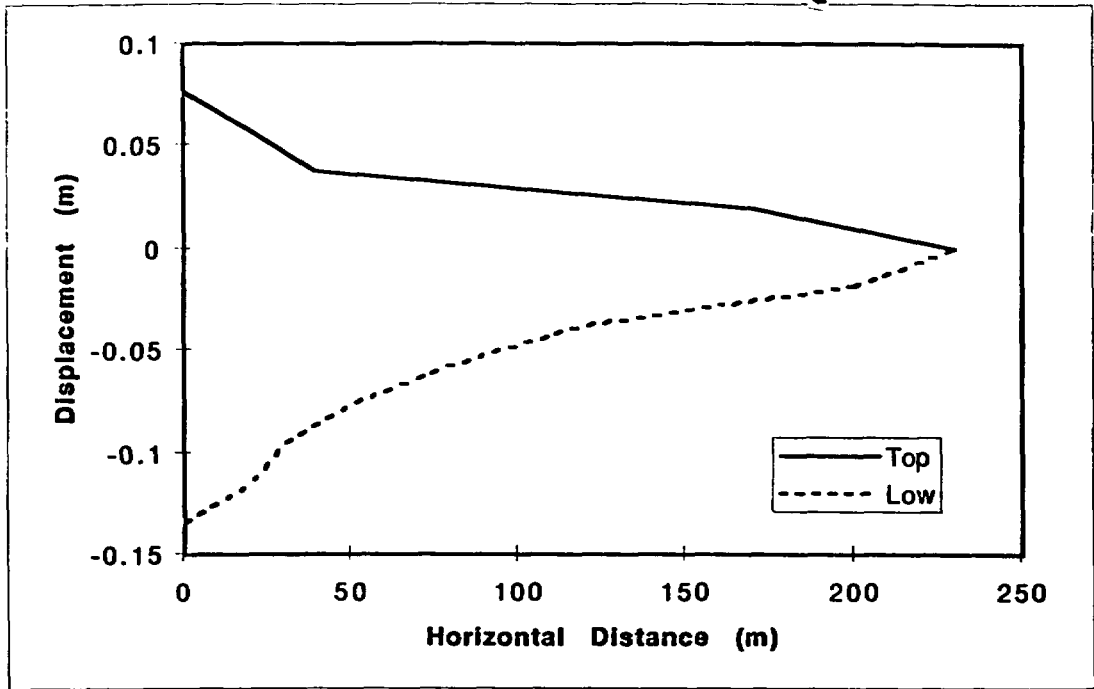


Figure 33. Fault displacement normal to the dip at depth = 5 km and dip = 50 degrees

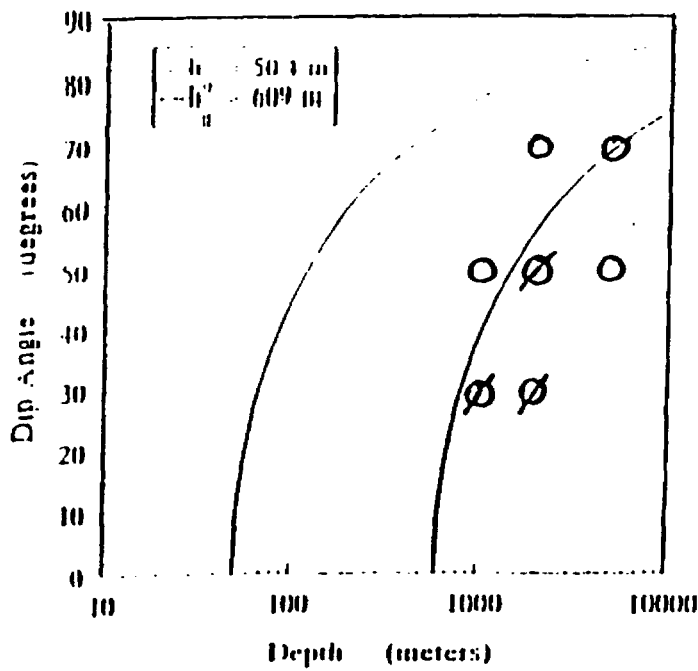


Figure 34. Summary of results from this study compared to theoretical curves shown in Figure 1. O indicates the fault opening > dike opening, Ø indicates the fault opening < dike opening